Photoinduced Multistep Energy and Electron Transfer in an Oligoaniline−Oligo(*p*-phenylene vinylene)−Fullerene Triad

Alicia Marcos Ramos,[†] Stefan C. J. Meskers,[†] Paul A. van Hal,[†] Joop Knol,[‡] J. C. Hummelen,[‡] and René A. J. Janssen*,[†]

Laboratory of Macromolecular and Organic Chemistry, Eindhoven University of Technology, PO Box 513, 5600 MB Eindhoven, The Netherlands, and Stratingh Institute and MSC, University of Groningen, Nijenborgh 4, 9747 AG Groningen, The Netherlands

Received: June 3, 2003; In Final Form: September 5, 2003

A donor−donor−acceptor triad, OAn−OPV−C_{60}, with a redox gradient has been synthesized by covalently linking an oligoaniline (OAn), an oligo(*p*-phenylene vinylene) (OPV), and a fullerene (C_{60}) in a nonconjugated linear array. Photoluminescence and femtosecond pump−probe spectroscopy studies reveal that photoexcitation of any of the three chromophores of this triad in a polar solvent results in formation of the OAn−OPV^+−C_{60}^- charge-separated state, after an efficient ultrafast (<190 fs) singlet-energy transfer to the fullerene singlet-excited state. The initial OAn−OPV^+−C_{60}^- state can rearrange to the low-energy OAn^+−OPV−C_{60}^- charge-separated state via an intramolecular redox reaction. Because the competing charge recombination of the OAn−OPV^+−C_{60}^- state to the ground state is fast and increases with increasing polarity of the solvent, the quantum yield for this charge shift is the highest (∼0.4) in weakly polar solvents such as chlorobenzene. Once formed, the OAn^+−OPV−C_{60}^- state has a long lifetime (>1 ns) due to weak electronic coupling between the distant redox sites in the excited state. The stabilization gained is more than 1 order of magnitude in time. The experimental results are found to be in qualitative agreement with Marcus theory. In thin films, the OAn^+−OPV−C_{60}^- state is formed at a higher rate and in higher quantum yield than in solution.

Introduction

Photoinduced energy and electron-transfer reactions are the key steps in natural photosynthesis, and the elucidation of their mechanism continues to attract considerable interest.[1] Similar processes occur in artificial photoactive and redoxactive molecular donor entities linked to acceptors. These systems are considered to be promising for applications in molecular and supramolecular electronics, light harvesting, and photocatalysis.[2] Molecular donor−acceptor combinations also find application in organic and polymer photovoltaic cells to convert sunlight into electrical energy.[3,4] One of the potentially promising materials for photovoltaic cells is a blend of a conjugated polymer as a donor and a methanofullerene derivative as the acceptor.[5] In these polymer:C_{60} bulk heterojunctions, the forward electron transfer is extremely fast (≪1 ps),[6] whereas the electron recombination extends to the millisecond time domain.[7] The large difference between the forward and backward transfer rates ensures efficient charge generation and gives the opportunity to transport and collect the photogenerated charges at the electrodes, and both processes have been studied extensively in recent years.

In this context, there is a considerable interest in the study of photoinduced charge generation in covalently linked dyads, consisting of linear conjugated oligomers and fullerenes.[8−12] Compared to the polymer:C_{60} blends, these covalently molecular dyads are much more well-defined and allow the charge-transfer reactions to be studied in different media. Using this approach, we showed that photoexcitation of the oligo(*p*-phenylene vinylene) unit of an OPV−C_{60} dyad (Figure 1) in a polar organic solvent results in an ultrafast (<190 fs) singlet-energy transfer (^{1}OPV*−C_{60} → OPV−$^1C_{60}$*), followed by a much slower (∼10 ps) electron-transfer reaction (OPV−$^1C_{60}$* → OPV^+−C_{60}^-) that produces a charge-separated state with a lifetime of 50 ps.[9e] More recent studies revealed that the rate of the forward electron-transfer reaction strongly depends on the relative orientation of the two moieties.[13] For an end-to-end substitution of donor and acceptor, the electron transfer is much slower (∼10 ps) than for a face-to-face orientation (≪1 ps), suggesting that the latter configuration explains the fast forward reaction observed in polymer:C_{60} blends. With respect to charge recombination, however, there remains a substantial discrepancy between the lifetimes of oligomer−C_{60} dyads in solution, which are typically less than 100 ps, and the long-lived charges in polymer:C_{60} films. Nature solved the problem of fast charge recombination in photosynthesis by creating a multistep electron transfer to increase the distance between the charges and slow recombination.[1] In mimicking natural photosynthesis, a number of multisite covalently linked porphyrin-fullerene combinations (triads, tetrads, and pentads) have been described,[14,15] showing that also in artificial fullerene systems multistep charge-transfer results in an increase in lifetime of the charge-separated state. Hence, inspired by nature, a tentative explanation for the long lifetime in the polymer:C_{60} films is the diffusion of charges to different sites in the blend.

In this contribution, we intend to connect the complementary views that originate from mimicking natural photosynthesis and polymer:C_{60} solar cells by extending the OPV−C_{60} dyad to include a *p*-oligoaniline (OAn) moiety as an additional donor, to create a donor−donor−acceptor triad (OAn−OPV−C_{60},

* To whom correspondence should be addressed. Phone: (+)31.40.2473597. Fax: (+)31.40.2451036. E-mail: r.a.j.janssen@tue.nl.
[†] Eindhoven University of Technology.
[‡] University of Groningen.

10.1021/jp035549+ CCC: $25.00
Published on Web 10/11/2003

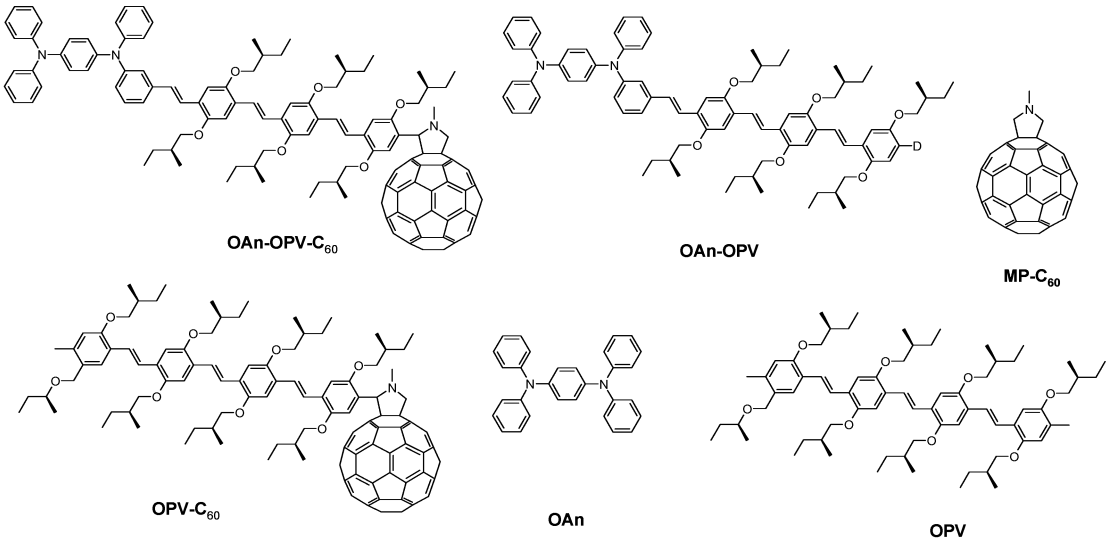

Figure 1. Structure of the OAn−OPV−C_{60} triad and reference compounds.

Figure 1). By using a meta substituted phenylene ring in OAn−OPV−C_{60}, the OAn and OPV parts are electronically decoupled in the ground state and operate as isolated redox active segments. In OAn−OPV−C_{60}, the oxidation potential decreases from C_{60}, via OPV, to OAn, while at the same time the reduction potential increases (vide infra). By introducing this redox gradient, we expect that the energetically most favorable charge-separated state corresponds to OAn^+−OPV−C_{60}^- and that the lifetime of this state is enhanced as a result of the larger distance between the centers of positive and negative charge density. The detailed analysis of the photophysical processes in OAn−OPV−C_{60} has been performed using photoluminescence and femtosecond pump−probe spectroscopy in solvents of different polarity and in the solid state and by comparing the results with those of the model compounds OAn−OPV, OPV−C_{60}, OPV, OAn, and MP−C_{60} (Figure 1) that have only one or two chromophores.

Results and Discussion

Synthesis. The synthesis of OAn,[16] OPV, MP−C_{60}, and OPV−C_{60}[9d] have been described elsewhere. The synthesis of the triad OAn−OPV−C_{60} (**7**, Scheme 1) starts from OPV aldehyde **1**, which has been described previously.[9d] The aldehyde functionality of **1** was protected as a dimethyl acetal **2**. Aldehyde **4** was obtained after reacting amine **3** with 3-bromobenzaldehyde in a palladium-catalyzed reaction. Aldehyde **4** was subsequently converted into the Schiff base **5** after refluxing with aniline in ethanol. *N*-Phenylaldimine **5** was then reacted with the methyl group of **2** in a Siegriest reaction[17] affording, after acidic work up, aldehyde **6**. A chlorobenzene solution of aldehyde **6**, *N*-methylglycine, and C_{60} was stirred for 16 h in the dark at reflux temperature to yield a mixture of C_{60}, the desired monoadduct, and higher adducts. The triad **7** was isolated after extensive column chromatography in a 43% yield. For the synthesis of the OAn−OPV dyad (**10**, Scheme 2), the bromine atom in **8** was exchanged for a deuterium atom by lithiation and subsequent deuteration with D_2O to yield **9**. A Siegriest reaction of **9** with *N*-phenylaldimine **5** afforded **10**. All compounds used in the photophysical investigations were fully characterized using ^1H and ^{13}C NMR spectroscopy, mass spectrometry, FT-IR, and elemental analysis.

UV/Visible Absorption. The absorption spectrum of OAn−OPV−C_{60} in toluene solution (Figure 2) exhibits two strong absorption bands at 327 and 440 nm and a weak absorption at 705 nm. Whereas each of the three chromophores contributes to the absorption band at 327 nm, the absorption at 440 nm is dominated by the $\pi-\pi^*$ transition of the OPV segment. The absorption at 705 nm is characteristic for fulleropyrrolidines.[9d] The absorption spectrum of OAn−OPV−C_{60} is a near superposition of the absorption spectra of the different components of the triad; only at high energies there is a slight deviation of the linear combination (Figure 2). This is likely due to the fact that the OAn−OPV−C_{60} triad has one less alkoxy substituted phenylene group compared to combined chromophores (OAn + OPV + MP−C_{60}).

Electrochemistry. The OAn−OPV−C_{60} triad exhibits a reversible first reduction wave at −0.70 V, corresponding to the fullerene moiety and three reversible oxidation waves due to the OAn (+0.55 V and +1.03 V) and the OPV (+0.83 V) moieties (potentials are given vs SCE, calibrated against Fc/Fc^+, recorded in dichloromethane with 0.1 M $TBAPF_6$) (Table 1). These oxidation potentials are in close agreement with the values established for the reference compounds (Table 1).[9d] The small difference in oxidation potential between the OPV moiety in triad OAn−OPV−C_{60} (+0.83 V) and the OPV chromophore (+0.78 V)[9d] is attributed to the smaller number of electron donating alkoxy substituents of the former. The reduction potentials of OPV and OAn−OPV (−1.91 and −1.87 V) were measured in tetrahydrofuran (THF) and are much more negative than that of the fullerene (Table 1).

Absorption Spectra of Redox States. UV/visible/near-IR spectroscopy enables the electronic transitions of the donor−acceptor arrays to be monitored during a stepwise oxidation process. Quantitative chemical oxidation of the OAn−OPV dyad in dichloromethane solution was achieved by the addition of thianthrenium perchlorate[18] (Figure 3). After the addition of one equivalent of this oxidizing agent, the intensity of the absorption band at 3.79 eV decreases and two absorption bands emerge in the spectrum, one at 1.44 eV and the other overlapping with the absorption band of the OPV unit at 2.83 eV. Comparison with the electronic transitions of the *N*,*N*,*N*',*N*'-tetraphenyl-1,4-benzenediamine radical cation (1.44 and 3.05 eV)[19] demonstrates that the absorption bands are associated with the formation of an OAn^+ radical cation, whereas the disappearing band is that of the neutral OAn moiety. When a second equivalent of thianthrenium perchlorate is added, the band of the neutral OPV unit, at 2.83 eV, decreases, and two absorption bands with

SCHEME 1. Synthesis of OAn−OPV−C_{60} (7)[a]

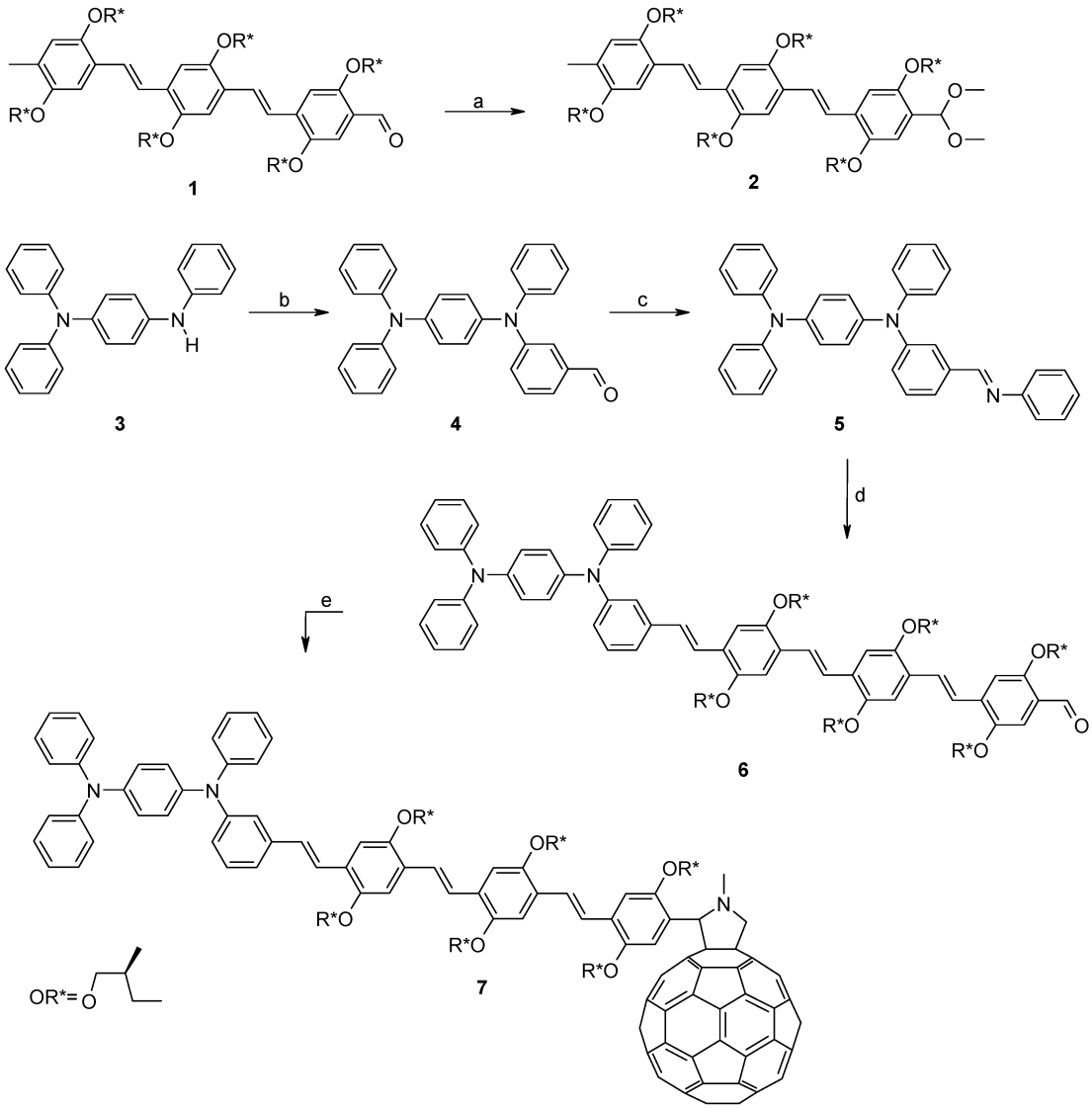

[a] a = amberlite IR 120, trimethyl orthoformate, methanol, 70 °C, 2 H, 91%. b = 3-bromobenzaldehyde, $Pd_2(dba)_3$, BINAP, Cs_2CO_3, toluene, 100° C, 5 days, 62%. c = aniline, ethanol, 85 °C, 4 H, 79%. d = 1. compound **2**, *t*-BuOK, DMF, 80° C, 5 H, 72%; 2. HCl. e = *N*-methylglycine, C_{60}, chlorobenzene, reflux, 18 H, 43%.

SCHEME 2. Synthesis of OAn−OPV (10)[a]

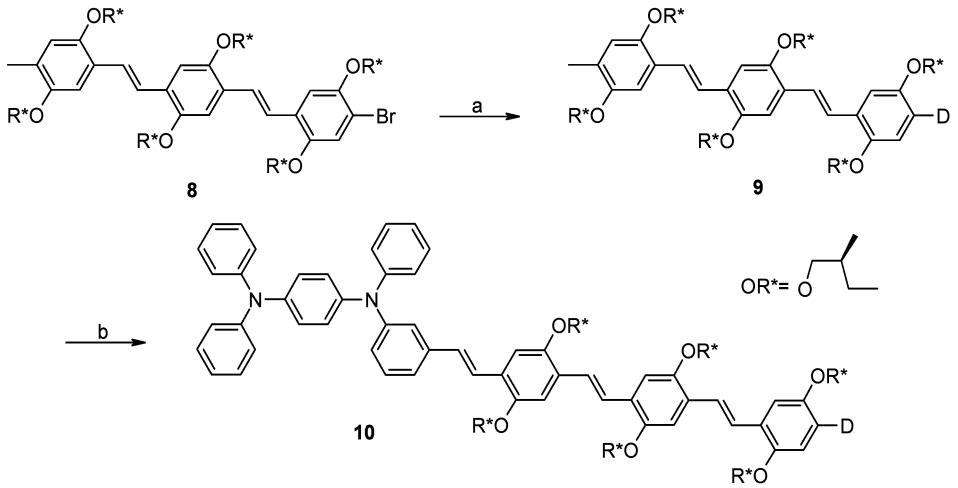

[a] a = 1. *n*-BuLi, diethyl ether, −10 °C; 2. D_2O, room temperature, 41%. b = 1. compound **5**, *t*-BuOK, DMF, 80° C, 3 H, 50%; 2. HCl.

vibronic fine structure, at 0.74 and 1.64 eV, related to an OPV^+ radical cation,[20] appear in the spectrum. At the same time, the absorption of OAn^+ at 1.44 eV remains and the second band of OAn^+ at 3.04 eV is now clearly observable. After two

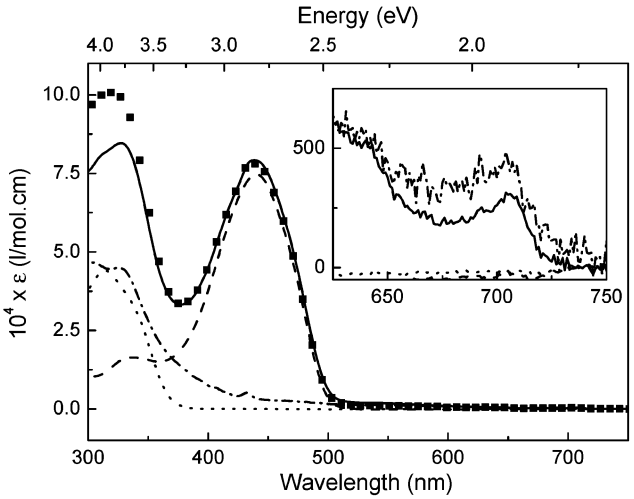

Figure 2. UV−visible absorption spectra of the OAn−OPV−C_{60} triad (solid line) and model compounds OAn (dotted line), OPV (dashed line), and MP−C_{60} (dashed−dotted line) recorded in toluene solution, and the summation of the spectra of all three reference compounds (squares). Inset: Magnification of the 705 nm absorptions.

TABLE 1: One-Electron Redox Potentials (E^0) of OAn, OPV, MP−C_{60}, OAn−OPV, and OAn−OPV−C_{60} (vs SCE) Calibrated with Fc/Fc$^+$ (in Dichloromethane with 0.1 M $TBAPF_6$)

compound	E^0_{red} (V)	E^0_{ox} (V)
OAn		0.53/1.02
OPV	−1.91[a]	0.78
MP−C_{60}	−0.70	
OAn−OPV	−1.87[a]	0.53
OAn−OPV−C_{60}	−0.70	0.53/0.83/1.03

[a] Measured in THF.

equivalents of oxidizing agent, the absorption spectrum exhibits the characteristics of both OAn^+ and OPV^+ radical cations and therefore corresponds to that of the OAn^+−OPV^+ dication diradical.

Energetic Considerations. In the two dyads (OAn−OPV, OPV−C_{60}) and triad (OAn−OPV−C_{60}), numerous processes may occur after photoexcitation. Apart from the intrinsic decay of the singlet-excited state of the individual chromophores (photoluminescence, intersystem crossing, and thermal decay), energy and electron-transfer reactions involving more than one chromophore (or redox active group) are possible. Whether these reactions occur depends on, among others, whether these processes are exergonic. The absorption spectra (Figure 2) reveal that the lowest singlet-excited state is located on the fullerene at 1.76 eV, followed by the singlet state of the OPV at 2.48 eV, whereas that of the OAn segment is positioned at approximately 3.40 eV.

The energies of the charge-separated states can be estimated by calculating the change in free energy ($\Delta G°$) for charge separation using a continuum model:[21]

$$\Delta G° = e(E_{ox}(D) - E_{red}(A)) - E_{00} - \frac{e^2}{4\pi\epsilon_0\epsilon_s R_{cc}} - \frac{e^2}{8\pi\epsilon_0}\left(\frac{1}{r^+} + \frac{1}{r^-}\right)\left(\frac{1}{\epsilon_{ref}} - \frac{1}{\epsilon_s}\right) \quad (1)$$

In this equation, $E_{ox}(D)$ and $E_{red}(A)$ are the oxidation and reduction potentials of the donor and acceptor molecules or moieties measured in a solvent with relative permittivity ϵ_{ref}, E_{00} is the energy of the excited state from which the electron transfer occurs, and R_{cc} is the center-to-center distance of the

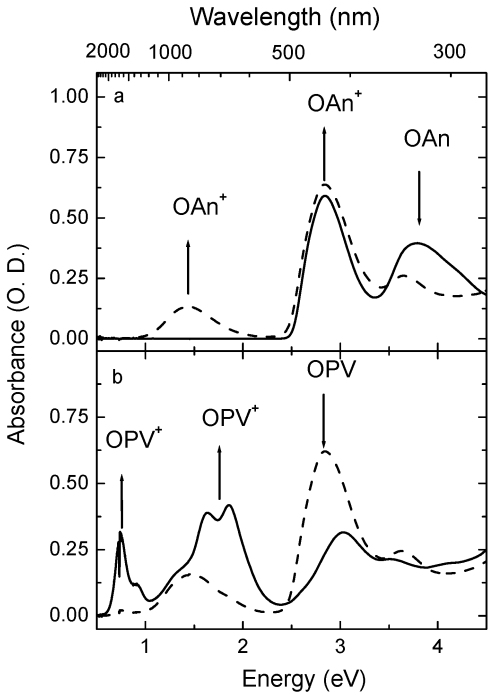

Figure 3. UV/visible/near-IR spectra recorded during the conversion of OAn−OPV by stepwise oxidation using thianthrenium perchlorate[18] in CH_2Cl_2: (a) before (solid line) and after (dashed line) adding 1 equiv. and (b) after adding 1 equiv. (dashed line) and 2 equiv. (solid line).

positive and negative charges in the charge separated state. The radii of the positive and negative ions are given by r^+ and r^-, and ϵ_s is the relative permittivity of the solvent, $-e$ is the elemental charge, and ϵ_0 is the vacuum permittivity. The R_{cc} distances were determined by molecular modeling, assuming that the charges are located at the centers of the OAn, OPV, and C_{60} moieties.[22] The radius of the negative ion of C_{60} was set to $r^- = 5.6$ Å and that of the ions of OPV to $r^+/r^- = 5.1$ Å.[9d] The radius of the positive charge of OAn was set to $r^+ = 4.8$ Å, as estimated from molecular modeling.

The change in free energy for charge separation was calculated for four solvents of interest with increasing polarity: toluene ($\epsilon = 2.38$), chlorobenzene ($\epsilon = 5.71$), *o*-dichlorobenzene ($\epsilon = 9.93$), and benzonitrile ($\epsilon = 25.2$) (Table 2). According to eq 1, charge separation (CS: OAn−OPV−$^1C_{60}$* → OAn−OPV^+−C_{60}^-) and the charge shift (CSH: OAn−OPV^+−C_{60}^- → OAn^+−OPV−C_{60}^-) are energetically feasible in the three polar solvents (Table 2).

The experimental and estimated energies of the various neutral and charge-separated states of the OAn−OPV−C_{60} triad are depicted in Figure 4, assuming chlorobenzene as the medium. Figure 4 also shows the prevailing photophysical reactions that have been identified (vide infra) in the triad or its model compounds.

Photoluminescence. Photoluminescence (PL) experiments on the triad, dyads, and model compounds were used to study the energy and electron-transfer reactions that occur in these molecules. These transfer relaxation pathways are expected to quench the PL of the chromophores, especially when their rate constants are higher than that of the intrinsic decay.

The PL at 499 nm of the OPV moiety (excitation at 440 nm) of the OAn−OPV−C_{60} triad, dissolved in toluene, is highly quenched (quenching factor $Q > 4000$) compared to the PL of the corresponding OPV molecule. Apart from a residual emission at 499 nm,[23] photoexcitation of the OPV moiety of OAn−OPV−C_{60} results in a weak PL signal at 715 nm (Figure

TABLE 2: Change in Free Energy (ΔG^0) with Reference to the Lowest Singlet State, Reorganization Energy (λ), and Barrier ($\Delta G^{\ddagger}$) for Charge Separation (CS), Charge Recombination (CR1), Charge Shift (CSH), and Charge Recombination (CR2) in Toluene (TOL), Chlorobenzene (CB), *o*-Dichlorobenzene (ODCB), and Benzonitrile (BZN) as Determined Using Eqs 1 and 2

reaction	solvent	ΔG^0 (eV)	λ (eV)	$\Delta G^{\ddagger}$ (eV)
OAn−OPV−$^1C_{60}$* → OAn−OPV$^+$−C_{60}^-	TOL	0.21	0.35	0.224
CS	CB	−0.22	0.75	0.093
	ODCB	−0.36	0.86	0.073
	BZN	−0.46	0.99	0.070
OAn−OPV$^+$−C_{60}− → OAn−OPV−C_{60}^-	TOL	−1.97	0.35	1.905
CR1	CB	−1.54	0.75	0.204
	ODCB	−1.40	0.86	0.088
	BZN	−1.30	0.99	0.024
OAn−OPV$^+$−C_{60}− → OAn$^+$−OPV−C_{60}^-	TOL	−0.08	0.35	0.051
CSH	CB	−0.21	0.80	0.106
	ODCB	−0.25	0.91	0.119
	BZN	−0.29	1.06	0.140
OAn$^+$−OPV−C_{60}^- → OAn−OPV−C_{60}	TOL	−1.89	0.36	1.618
CR2	CB	−1.32	0.89	0.053
	ODCB	−1.15	1.03	0.004
	BZN	−1.01	1.20	0.007
OAn−^{1}OPV* → OAn$^+$−OPV$^-$	TOL	0.41	0.35	0.407
CS	CB	−0.07	0.80	0.165
	ODCB	−0.22	0.91	0.133
	BZN	−0.34	1.06	0.123

5a), characteristic of the fluorescence emission band of fulleropyrrolidines.[9d] In toluene, the quantum yield of this emission is nearly identical to that of the reference compound MP−C_{60}. The same result is observed for the OPV−C_{60} dyad, although in this case the PL quenching of the OPV is somewhat less ($Q \approx 1500$).[23] The strong quenching of the ^{1}OPV* singlet-excited state (S_1) in the OPV−C_{60} dyad has previously been studied in detail and was found to involve an ultrafast photoinduced intramolecular singlet-energy transfer (ET) toward the fullerene moiety (^{1}OPV*−C_{60} → OPV−$^1C_{60}$*), which occurs with a time constant of less than 190 fs.[9e,24] We propose that the same ET process occurs in the OAn−OPV−C_{60} triad. In accordance with this proposition, the excitation spectrum of the fullerene fluorescence of OAn−OPV−C_{60} coincides with the corresponding absorption spectrum of OAn−OPV−C_{60} (Figure 5b). It is interesting to note that the fullerene excitation spectra of OPV−C_{60} and OAn−OPV−C_{60} differ appreciably at lower wavelengths, where the OAn moiety absorbs. The excellent agreement between the absorption spectrum of the OAn−OPV−C_{60} triad and the excitation spectrum of the fullerene fluorescence of the triad implies that not only excitation of OPV, but also excitation of OAn is responsible for the emission of the fullerene. This points to an efficient sequential singlet-energy transfer in the triad (Figure 4), which starts with the formation of the ^{1}OAn*−OPV−C_{60} singlet-excited state and ends at the OAn−OPV−$^1C_{60}$* fullerene singlet-excited state.

In a more polar solvent, like *o*-dichlorobenzene ($\epsilon = 9.93$), the PL of the OPV unit of the OAn−OPV−C_{60} triad is quenched to a similar extent as in toluene (Figure 5a). In contrast, the PL of the fullerene moiety at 715 nm is significantly quenched in this more polar solvent as compared to in toluene (Figure 5a). The same result has previously been observed for the OPV−C_{60} dyad[9d,e] and gives evidence of a photoinduced charge separation (CS) that occurs from the fulleropyrrolidine singlet-excited state and produces the OPV$^+$−C_{60}^- charge-separated state. For the OAn−OPV−C_{60} triad, a photoinduced CS will initially produce a similar state (OAn−OPV$^+$−C_{60}^-), which may then go through a charge shift (CSH) to generate the energetically more favorable OAn$^+$−OPV−C_{60}^- state (Figure 4).

For a further comparison, we have studied the PL of the OAn−OPV dyad in solvents of different polarity. Figure 6a shows that the emission of ^{1}(OAn−OPV)*, dissolved in toluene, stems exclusively from the OPV moiety, irrespective of the excitation wavelength (330 nm (OAn) or 444 nm (OPV)). This implies that an efficient singlet-energy transfer occurs from the excited ^{1}OAn* state to OPV (^{1}OAn*−OPV → OAn−^{1}OPV*). In toluene, the fluorescence quantum yield of OAn−OPV is slightly (∼10%) higher than that of OPV, but the PL is progressively quenched with increasing solvent polarity (Figure 6a), providing quenching factors of $Q \approx 2$, 9, and 22 for chlorobenzene, *o*-dichlorobenzene, and benzonitrile, respectively. The quenching of OAn−OPV PL after excitation at 440 nm in more polar solvents is attributed to an intramolecular photoinduced electron-transfer reaction in the excited state to produce the OAn$^+$−OPV$^-$ state. The excitation spectrum of the residual emission of OAn−OPV recorded in chlorobenzene (Figure 6b) closely corresponds to the absorption spectrum of OAn−OPV. This indicates that the ^{1}OAn*−OPV → OAn−^{1}OPV* singlet-energy transfer is significantly faster than an electron transfer from the same state (^{1}OAn*−OPV → OAn$^+$−OPV-). Hence, OAn$^+$−OPV$^-$ is primarily formed via the OAn−^{1}OPV* singlet state, irrespective of the excitation wavelength.

Near Steady-State Photoinduced Absorption (PIA) Spectroscopy. Near steady-state PIA spectroscopy in the microsecond and millisecond time domain is a very sensitive technique (detection limit $\Delta T/T \sim 10^{-6}$) to probe small concentrations of long-lived photoexcitations such as triplet states and intermolecular charge-separated states. The PIA spectrum of OAn−OPV−C_{60} in toluene solution, recorded with excitation at 458 nm, exhibits a band at 1.78 eV with a shoulder at 1.52 eV, characteristic of the long-lived (∼40 μs) triplet state of the fulleropyrrolidine moiety (OAn−OPV−$^3C_{60}$*) formed via intersystem crossing from the fullerene singlet-excited state. [9d]

The photoinduced electron transfer in OAn−OPV−C_{60} in *o*-dichlorobenzene and subsequent charge shift or charge recombination will likely occur in the picosecond to nanosecond time regime and cannot be resolved with the near-steady-state PIA technique. However, absorptions of the charge-separated states can be observed in mixtures of the different model compounds of the triad in *o*-dichlorobenzene solution, by using the redox activity of the corresponding triplet states. Photoexcitation of OPV (at 458 nm) or MP−C_{60} (at 528 nm) will result in the formation of the corresponding excited triplet states. These triplet states (^{3}OPV* and MP−$^3C_{60}$*) can undergo an electron transfer to one of the other redox active chromophores present in solution to produce an intermolecularly charge-separated state, which is long-lived because the formed cation and anion radicals diffuse away in solution.

Accordingly, selective photoexcitation of MP−C_{60} at 528 nm in mixtures with OPV or OAn in *o*-dichlorobenzene solution produces the charge-separated states OPV$^+$/MP−C_{60}^- and OAn$^+$/MP−C_{60}^-, respectively, which are characterized by the absorptions of OPV$^+$ (at 0.68 and 1.52 eV), OAn$^+$ (at 1.40 eV), and MP−C_{60}^- (at 1.24 eV) (Figure 7a). Likewise, photoexcitation of MP−C_{60} in a mixture with OAn−OPV in *o*-dichlorobenzene results in a band at 1.40 eV (Figure 7b) attributed to the OAn$^+$−OPV radical cation. Although in this mixture the OAn−OPV$^+$ radical cation can also be formed, it will probably rearrange by an intramolecular redox reaction to the OAn$^+$−OPV state within the time scale of the experiment. In an equimolar mixture of OAn, OPV, and MP−C_{60}, charge transfer from the positively charged OPV$^+$ onto the OAn becomes intermolecular, i.e., diffusion-limited and slower. This allows

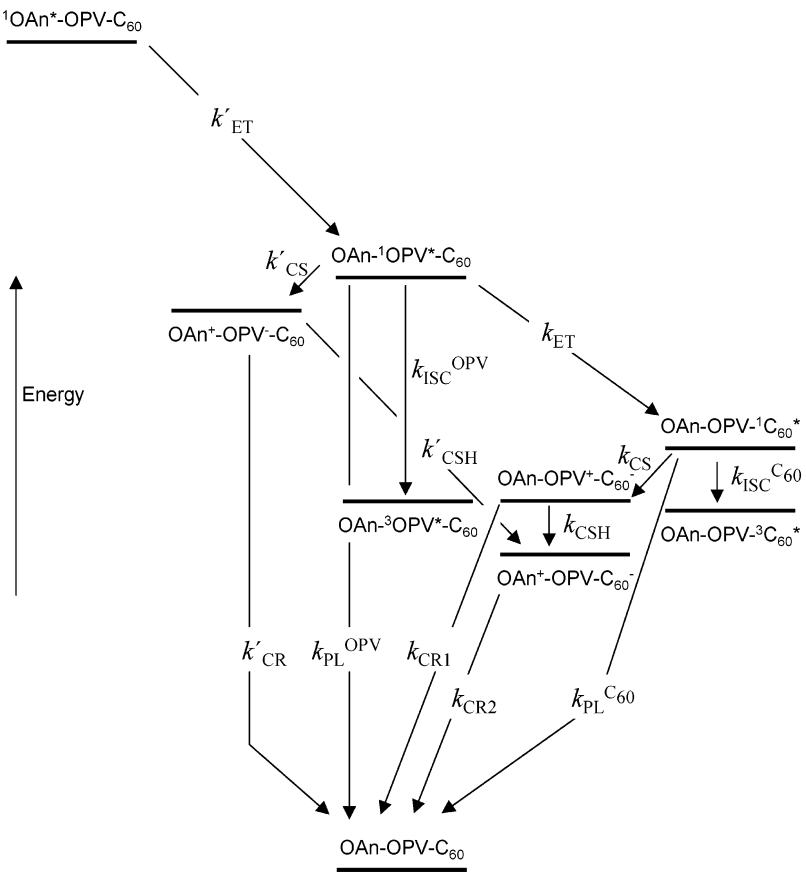

Figure 4. Schematic energy levels (in chlorobenzene) and photoinduced processes in OAn−OPV−C_{60}. The rate constants are collected in Table 3.

for the detection of a weak residual absorption band characteristic of the OPV^+ radical cation in the PIA spectrum at 0.68 eV (Figure 7b).

Even in a mixture where both OPV and MP−C_{60} are present in 4-fold excess with respect to OAn, the PIA spectrum is still dominated by the absorption of the OAn^+ radical cation (Figure 7c). At high modulation frequency (2500 Hz) the relative intensity of the OPV^+ radical cation band at 0.68 eV increases compared to low modulation frequency (75 Hz) (when normalized at 1.24 eV), indicating that in this mixture OPV^+ has a shorter lifetime than the OAn^+ radical cation, consistent with the proposed $OPV^+ + OAn \rightarrow OPV + OAn^+$ redox reaction.

Femtosecond Pump−Probe Spectroscopy in Polar Solvents. The formation and decay of the transient charged species generated after photoexcitation of the OPV moiety in OAn−OPV−C_{60} and the reference compounds OPV−C_{60} and OAn−OPV have been investigated with subpicosecond pump−probe spectroscopy in solvents of different polarity.

Upon excitation at 450 nm of OPV−C_{60} or OAn−OPV−C_{60}, the transient absorption at 1450 nm (0.85 eV) that is associated with the OPV^+ radical cation, i.e., the $OPV^+-C_{60}^-$ and $OAn-OPV^+-C_{60}^-$ states, exhibits a rise and a decay component (Figure 8). It is important to note that the charge separation occurs after the ultrafast singlet-energy transfer: $(OAn-)^1OPV^*-C_{60} \rightarrow (OAn-)OPV-{}^1C_{60}^*$ ($k_{ET} \geq 5.3 \times 10^{12}$ s^{-1}).[9e] Fitting of the temporal differential absorption data at 1450 nm to a biexponential function[25] provides the rate constants for forward and backward electron-transfer reactions (Table 3). As can be seen in Figure 8 (and Table 3), the rate constants for the charge separation (k_{CS}) are equal in the dyad and triad within experimental error. The rates for charge separation in the dyad and triad increase significantly with solvent polarity from $k_{CS} = 4.3 \times 10^{10}$ s^{-1} in chlorobenzene to $k_{CS} = 2.0 \times 10^{11}$ s^{-1} in benzonitrile. A similar increase is found for the charge recombination. This effect of the medium on the rate constant has often been observed in donor−acceptor dyads and is in agreement with Marcus theory, vide infra.[26]

In comparison to the dyad, the charge shift (CSH) from $OAn-OPV^+-C_{60}^-$ to $OAn^+-OPV-C_{60}^-$ provides an extra pathway in the triad for the decay of the OPV^+ radical other than charge recombination (CR1, Figure 4) to the ground state. Hence, the OPV^+ radical cation absorption may disappear faster in the triad than in the dyad. The experimental data in Figure 8 show, however, that this difference is only discernible in chlorobenzene, i.e., the least polar solvent. This is a direct consequence of the increased rate for charge recombination in more polar solvents (Figure 8), which implies that the probability for the competing (slower) charge shift is strongly reduced. Nonlinear least-squares analysis of the experimental OPV^+ traces (Figure 8) does not give a clear indication of the magnitude of the rate of charge shift; it yields values of k_{CR1} and ($k_{CR1} + k_{CSH}$) that are essentially the same (see Table 3). This may be explained in part by a difference in k_{CR1} for the dyad and the triad and in part by the difficulties in the data analysis itself. Due to the fact that the rates for formation and decay of the OPV^+ species are very similar, it is difficult to estimate the rates, as nonlinear-least-squares-fit procedures tend to yield parameters, which are strongly correlated.

Additional information on the CSH reaction can be obtained by measuring the photoinduced absorption at 1030 nm (1.20 eV). At this probe wavelength, the S_1 states ^{1}OPV* and ^{1}MP−C_{60}*, as well as the radical ions MP−C_{60}^- and OAn^+, contribute

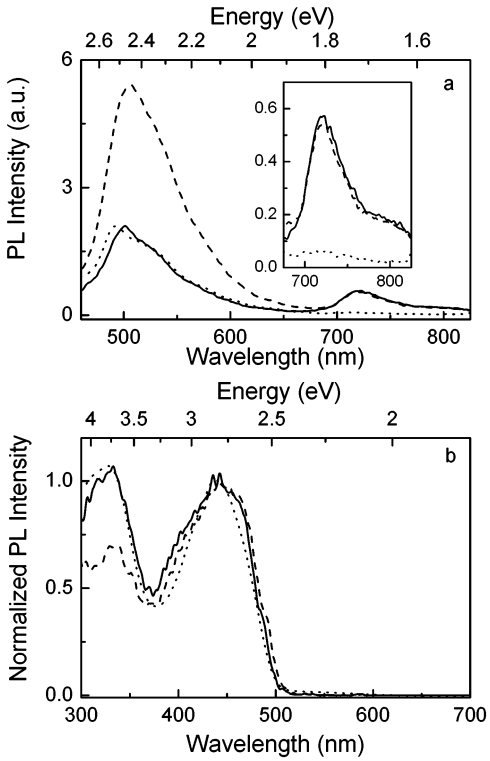

Figure 5. (a) PL spectra of OPV−C_{60} in toluene (dashed line) and of OAn−OPV−C_{60} in toluene (solid line) and *o*-dichlorobenzene (dotted line). The inset shows a magnification of the fullerene emission. (b) Excitation spectra of the 710 nm emission of OPV−C_{60} (dashed line) and OAn−OPV−C_{60} (solid line) compared to the absorption spectrum of OAn−OPV−C_{60} (dotted line), all in toluene.

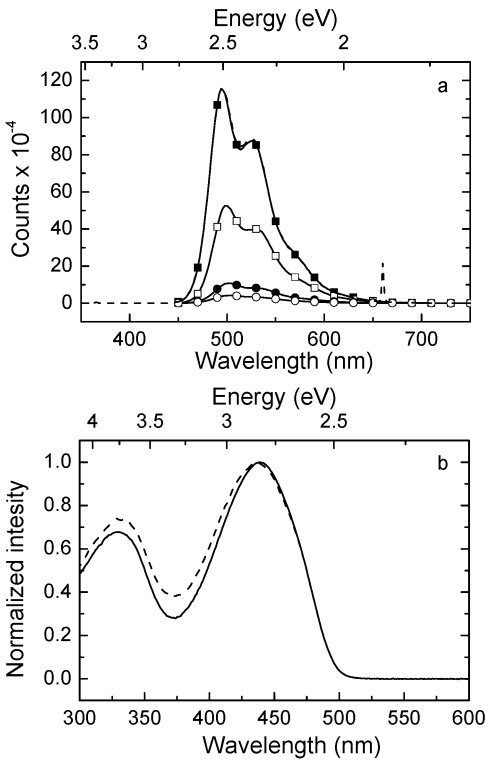

Figure 6. (a) PL spectra of OAn−OPVin toluene (solid squares), chlorobenzene (open squares), *o*-dichlorobenzene (closed circles), and benzonitrile (open circles) solutions with excitation at 444 and 330 nm (for toluene only, dashed line). (b) Excitation spectrum of the OPV emission at 500 nm of OAn−OPV in chlorobenzene (dashed line) and compared to the absorption spectrum (solid line).

to the induced absorption (Figure 7). The differential transmission at 1030 nm of OPV−C_{60} and OAn−OPV−C_{60} in chlorobenzene undergoes a strong rise and drop within 2 ps (Figure 9). This transient signal is associated with the formation and decay of the ^{1}OPV* singlet-excited state and involves the $S_n \leftarrow S_1$ transition of the OPV unit.[9e] The short lifetime of the ^{1}OPV* state is due to the ultrafast ET onto the fullerene moiety as described above. After the ET, the 1030 nm signal for the OAn−OPV−C_{60} triad remains constant over the time scale of the experiment (1 ns), whereas for the dyad, the signal decays to zero within 200 ps (Figure 9). We propose that the remaining signal is due to absorption by C_{60}^- and OAn^+ radical ions, and hence characteristic of the OAn^+−OPV−C_{60}^- charge separated state. Using the extinction coefficients in brackets for these species [7.7×10^4 M^{-1} cm^{-1} (OPV(S_1), estimate), 7×10^3 M^{-1} cm^{-1} (MP−C_{60}(S_1)[27]), 7×10^3 M^{-1} cm^{-1} (MP−C_{60}^- [27]), and 8.2×10^3 $M^{-1}cm^{-1}$ (OAn^+ [19])], we have modeled the time profile for the absorption at 1030 nm (Figure 9) for both the OPV−C_{60} dyad and the OAn−OPV−C_{60} triad. Rate constants were taken from the transient absorption measurements at 1450 nm probe wavelength (Table 3) and the rate for charge shift (k_{CSH}) is used as an adjustable parameter.[28] Further details of the mathematical modeling are given in the Supporting Information. The results show a large induced absorption due to the OPV(S_1) species. The duration of this transient is mainly determined by the width of the laser pulses used. For the modeling, a cross-correlation of 500 fs (fwhm) for the pump and probe pulse was assumed. For the dyad, a smooth trace is observed after the initial contribution of the excited OPV moiety. This is consistent with the fact that the C_{60}(S_1) and the C_{60}^- groups have almost equal extinction coefficients. For the triad, a long-lived signal is observed which can be modeled taking $k_{CSH} = 5 \times 10^9$ s^{-1} and $k_{CR1} = 6 \times 10^9$ s^{-1}. Taking a higher (lower) value for k_{CSH} results in a curve that bends downward (upward) after 60 ps. Using $k_{CSH} = 5 \times 10^9$ s^{-1} results in a calculated yield of formation for the OAn^+−OPV−C_{60}^- species of about 0.4 per absorbed photon. This result can be compared with the following crude estimate. At 30 ps, mainly the OAn^+−OPV^+−C_{60}^- state is present of which only the C_{60}^- makes a major contribution to the absorption at 1030 nm. At $t = 200$ ns, only the OAn^+−OPV−C_{60}^- state is present and OAn^+ and C_{60}^- contribute almost equally to the transient absorption. The experimental observation that the induced absorption at 1030 nm hardly changes between 30 and 200 ps thus indicates that the probability of formation of OAn^+−OPV−C_{60}^- out of OAn^+−OPV^+−C_{60}^- is roughly one-half, in good agreement with the estimate above. Figure 9 also shows the induced absorption signal at 1450 nm as observed for the triad. This latter signal has been modeled using the same parameters as mentioned above. The value of $k_{CR1} = 6 \times 10^9$ s^{-1} obtained for the triad can be compared to $k_{CR1} = 12 \times 10^9$ s^{-1} obtained for the dyad by probing the OPV^+ cation absorption. At present, we cannot fully account for this difference. The method used here to determine k_{CSH} has the advantage that it does not rely on rate parameters obtained from model compounds. For the other two solvents used (ODCB and BZN), a long-lived transient at 1030 nm has a weak intensity, and the signal-to-noise ratio does not allow for an estimate of the rate for charge shift.

We also studied the reference compound OAn−OPV with pump−probe spectroscopy in solution. In particular, it is of interest to investigate whether an OAn−^{1}OPV*−$C_{60} \rightarrow$ OAn^+−OPV^-−C_{60} electron-transfer reaction can compete with the OAn−^{1}OPV*−$C_{60} \rightarrow$ OAn−OPV−$^1C_{60}$* energy transfer.

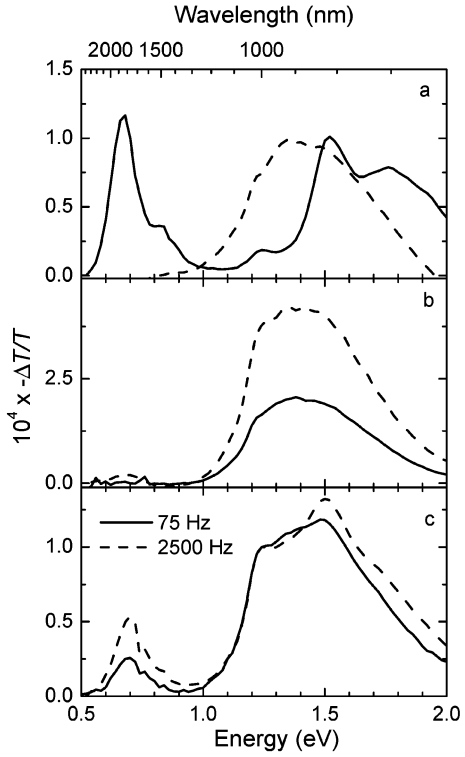

Figure 7. (a) Normalized photoinduced absorption spectra of the mixtures OPV/MP−C_{60} (1:1) (solid line) and OAn/MP−C_{60} (1:1) (dashed-line) in *o*-dichlorobenzene (excitation at 528 nm with 25 mW and modulation frequency of 275 Hz). (b) Photoinduced absorption spectra of the mixtures OAn−OPV/MP−C_{60} (1:1) (solid line) or OAn/OPV/MP−C_{60} (1:1:1) (dashed line) in *o*-dichlorobenzene (excitation at 528 nm with 25 mW and modulation frequency of 275 Hz). (c) Normalized photoinduced absorption spectra of the mixture OAn/OPV/MP−C_{60} (1:4:4) in *o*-dichlorobenzene recorded at modulation frequencies of 75 Hz (solid line) and 2500 Hz (dashed line) (excitation at 528 nm with 25 mW).

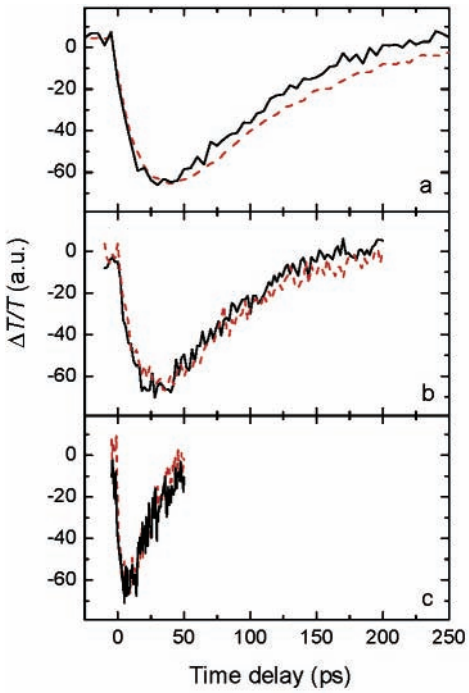

Figure 8. Differential transmission dynamics of the OPV^+ transition at 1450 nm for OAn−OPV^+−C_{60}^- (solid line) and OPV^+−C_{60}^- (dashed line) in (a) chlorobenzene, (b) *o*-dichlorobenzene, and (c) benzonitrile after excitation at 450 nm.

As a result of the electron−hole symmetry in conjugated oligomers, the optical spectra of OPV radical cations and OPV radical anions are expected to be very similar, and hence, we probe the formation of OPV^- at 1450 nm.[29] The transient differential transmission recorded for OAn−OPV, dissolved in solvents with increasing polarity, at 1450 nm after excitation at 455 nm, is shown in Figure 10. In full agreement with the PL quenching of the OAn−OPV fluorescence (Figure 6), the OAn^+−OPV^- charge-separated state is only formed in the three polar solvents (chlorobenzene, *o*-dichlorobenzene, and benzonitrile) but not in (less polar) toluene (Figure 10). The rate constants for charge separation and charge recombination (k'_{CS} and k'_{CR}, Table 3) increase with increasing polarity. Table 3 reveals that the rate for the OAn−^{1}OPV* → OAn^+−OPV^- charge separation ($k'_{CS} = 1.6-4.1 \times 10^{10}$ s^{-1}) is significantly less than the rate of the ^{1}OPV*−C_{60} → OPV−$^1C_{60}$* energy transfer ($k_{ET} \geq 5.3 \times 10^{12}$ s^{-1}), and as a consequence, the OAn^+−OPV^-−C_{60} state is unlikely be to formed in a significant yield from OAn−^{1}OPV*−C_{60}. Hence, excitation of OAn−OPV−C_{60} in solution will always provide OAn−OPV−$^1C_{60}$* as an intermediate state, irrespective of the excitation wavelength and solvent polarity.

Charge recombination in OAn^+−OPV^- is almost an order of magnitude slower than in OPV^+−C_{60}^- and occurs in the nanosecond regime. In this respect, a remarkable phenomenon was observed when the fluorescence lifetimes of OAn−OPV were recorded. In the most polar solvents *o*-dichlorobenzene and benzonitrile, the lifetime of the OAn−OPV emission is significantly reduced to ∼140 and ∼100 ps, compared to that of the OPV model compound (1.36 and 1.44 ns, respectively). This is in accordance with the proposed OAn−^{1}OPV* → OAn^+−OPV^- electron-transfer reaction, which reduces the lifetime of the ^{1}OPV* state. The lifetimes of ^{1}OPV* and OAn−^{1}OPV* in toluene are very similar (1.20 and 1.38 ns, Figure 9) as expected because electron transfer does not occur here. However, and surprisingly, a significant increase of fluorescence lifetime was observed for OAn−^{1}OPV* in chlorobenzene (2.65 ns) compared to OPV (1.27 ns) (Figure 11). At first glance, this increase in fluorescence lifetime seems to contradict the observed OAn−^{1}OPV* → OAn^+−OPV^- charge separation reaction, which is approximately 20 times faster than the intrinsic decay (Figure 10, Table 3). Instead of an increase in fluorescence lifetime, a decrease would be expected. Note that except for a loss in intensity (only a factor of 2), the fluorescence spectra of OPV and OAn−OPV are identical (Figure 6) and that the emission is thus from the OAn−^{1}OPV* state. Taking these experimental observations into consideration, we propose that in chlorobenzene the singlet OAn−^{1}OPV* state and the OAn^+−OPV^- charge-separated state are nearly degenerate and that back electron transfer from OAn^+−OPV^- reproduces the OAn−^{1}OPV* singlet state. The estimated change in free energy for OAn−^{1}OPV* → OAn^+−OPV^- of only $\Delta G^0 = -0.07$ eV (Table 2) supports this suggestion.

Kinetic Considerations. The final outcome of a photoexcitation not only depends on the energetics of the reaction, but also on the kinetics. Marcus theory provides an estimate for the free energy barrier ($\Delta G^{\ddagger}$) for electron-transfer reactions based on the change in free energy (ΔG^0) and the reorganization energy (λ) via:

$$\Delta G^{\ddagger} = \frac{(\Delta G^0 + \lambda)^2}{4\lambda} \qquad (2)$$

The reorganization energy consists of an internal contribution

TABLE 3: Rate Constants for the Intrinsic Decay of the Lowest-Energy Singlet-Excited Chromophore (k_0^{OPV}, k_0^{C60}), Singlet-Energy Transfer (k_{ET}), Charge Separation (k_{CS}), Charge Recombination (k_{CR1}), and Charge Shift (k_{CSH}) in the Studied Compounds in Toluene (TOL), Chlorobenzene (CB), *o*-Dichlorobenzene (ODCB), Benzonitrile (BZN), and in the Solid State

compound		TOL k (ns^{-1})	CB k (ns^{-1})	ODCB k (ns^{-1})	BZN k (ns^{-1})	film k (ns^{-1})
OPV	k_0^{OPV}	0.83	0.79	0.74	0.69	
MP−C_{60}	k_0^{C60}	0.68	0.72	0.75	0.68	
OPV−C_{60}	k_{ET}	≥5300	n.d.	≥5300	n.d.	
	k_{CS}		40 ± 2	50 ± 9	250 ± 40	≥3000
	k_{CR1}		12 ± 1	19 ± 3	37 ± 8	1.1
OAn−OPV−C_{60}	k_{ET}	≥5300	n.d.	≥5300	n.d.	
	k_{CS}		48 ± 5	71 ± 12	201±54	≥3000
	$k_{CR1}+k_{CSH}$		11 ± 1	16 ± 3	61±19	49
OAn−OPV	k'_{CS}		16.4	15.6	40.8	
	k'_{CR}		1.0	1.4	4.1	

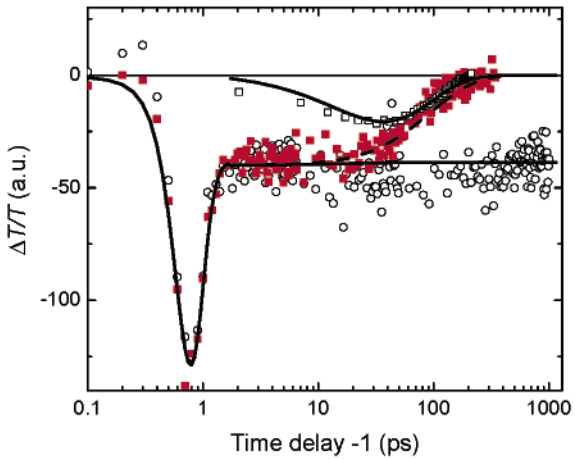

Figure 9. Differential transmission dynamics of OAn−OPV−C_{60} (open circles) and OPV−C_{60} (closed squares) in chlorobenzene monitored at 1030 nm with excitation at 450 nm. The induced absorption signal at 1450 nm as observed for the triad is shown with open squares. The lines correspond to a numerical simulation based on the model described in the text. For the simulation, the rate constants from Table 3 are used and the rate for charge shift is used as an adjustable parameter. The time delay has been shifted by 1 ps to show the signals on a logarithmic plot.

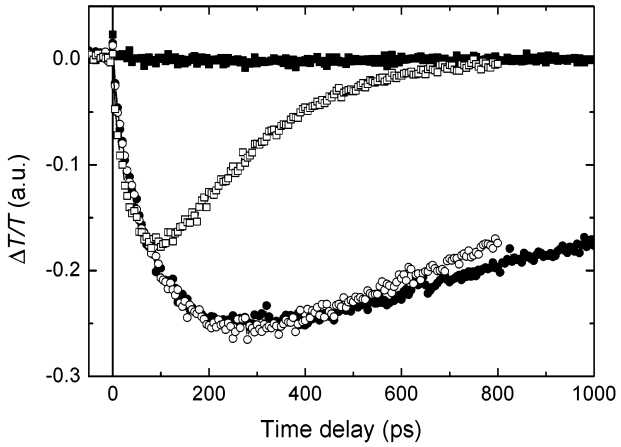

Figure 10. Differential transmission dynamics of OAn^+−OPV^- in toluene (closed squares), chlorobenzene (closed circles), *o*-dichlorobenzene (open circles), and benzonitrile (open squares) monitored at 1450 nm with excitation at 455 nm.

(λ_i) and a solvent term (λ_s), which can be approximated via the Born-Hush approach to give after summation

$$\lambda = \lambda_1 + \lambda_s = \lambda_i + \frac{e^2}{4\pi\epsilon_0}\left(\frac{1}{2}\left(\frac{1}{r^+}+\frac{1}{r^-}\right)-\frac{1}{R_{cc}}\right)\left(\frac{1}{n^2}-\frac{1}{\epsilon_s}\right) \quad (3)$$

The rate constants for the different processes are not only a function of the energy barrier $\Delta G^{\ddagger}$ but also of the reorganization energy (λ) and the electronic coupling (V) between donor and acceptor in the excited-state according to the equation

$$k = \left(\frac{4\pi^2}{h^2\lambda k_B T}\right)^{1/2} V^2 \exp\left[-\frac{(\Delta G^0+\lambda)^2}{4\lambda k_B T}\right] \quad (4)$$

The values of ΔG^0, λ, and $\Delta G^{\ddagger}$ calculated on the basis of eqs 1−4 collected in Table 2 show that the initial charge separation (k_{CS}) is in the Marcus normal region ($-\Delta G^0 < \lambda$). As the polarity of the solvent increases, the OAn−OPV^+−C_{60}^- charge-separated state is stabilized with a concomitant increase of the reorganization energy. The combination of these trends results in reduction of the barrier for charge separation in more polar solvents (Table 2). As a consequence, the rate for charge separation (k_{CS}) is expected to increase with polarity as has been found experimentally (Figure 8, Table 3). Charge recombination in OAn−OPV^+−C_{60}^- is in the Marcus inverted region ($-\Delta G^0 > \lambda$). The use of eq 4 in the inverted region often underestimates the true rate constant because of nuclear tunneling[30] but will be used here for qualitative comparison. We find that the barrier for charge recombination is strongly reduced in more polar solvents, consistent with the higher recombination rate (k_{CR1}, Table 3). Apart from recombination to the ground state, the OAn−OPV^+−C_{60}^- state may undergo a charge shift to form OAn^+−OPV−C_{60}^-. The charge shift occurs in the normal region ($-\Delta G^0 < \lambda$) and is energetically less favorable than the recombination (Table 3). However, in contrast to the recombination, the barrier for charge shift is reduced with decreasing polarity. Hence, the balance between charge recombination and the competing charge shift, will move toward the latter with decreasing polarity. As a result, the barrier for the charge shift

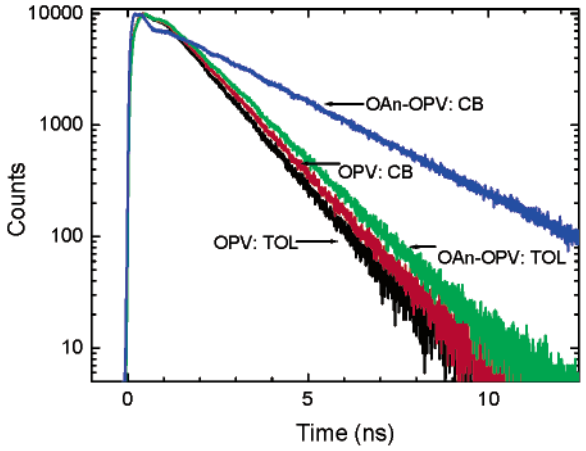

Figure 11. Time-resolved fluorescence of OPV and OAn−OPV in toluene (TOL) and chlorobenzene (CB) recorded with excitation at 400 nm.

TABLE 4: Relative Rate Constants for the Charge Separation (CS), Charge Recombination (CR1), Charge Shift (CSH), and Charge Recombination (CR2) in *o*-Dichlorobenzene (ODCB) and Benzonitrile (BZN) Compared to the Corresponding Rate Constant in Chlorobenzene (CB), Calculated Using Eq 4

relative rate constant	CS	CR1	CSH	CR2
k(CB)	1	1	1	1
k(ODCB)	2.00	89	0.58	6.25
k(BZN)	2.16	980	0.23	5.06

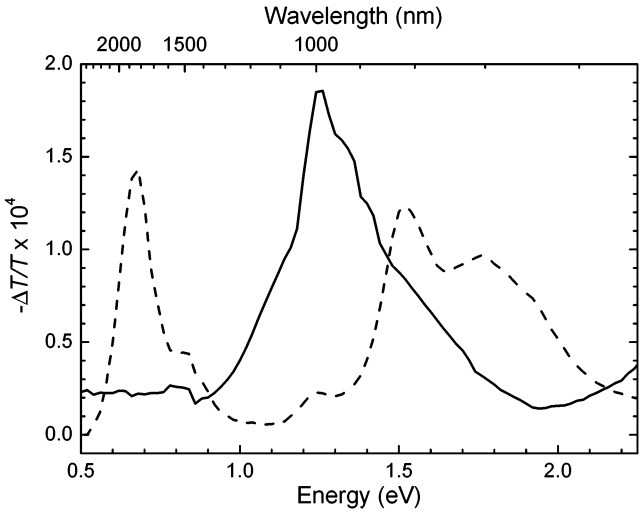

Figure 12. Photoinduced absorption spectra of OAn−OPV−C_{60} (solid line) and OPV−C_{60} (dotted line) in thin films. Recorded at 80 K with excitation at 458 nm (25 mW) and a modulation frequency of 275 Hz.

in OAn−OPV^+−C_{60}^- is lower than that for charge recombination in chlorobenzene but not in *o*-dichlorobenzene and benzonitrile. This is in full agreement with the experimental result that the charge shift was more easily observed in chlorobenzene (Figures 8 and 9).

The energy barriers for relaxation to the ground state in OAn^+−OPV−C_{60}^- are small. However, besides the energy barrier, the rate constant (eq 4) is also determined by the electronic coupling V. This electronic coupling depends exponentially on the center-to-center distance between the donor and acceptor via $V^2 = V_0^2(R_0)\ \exp(-\beta(R_{cc} - R_0))$, with R_0 the contact distance. Hence, V is orders of magnitude less for OAn^+−OPV−C_{60}^- ($R_{cc} = 30.0$ Å) than for OAn−OPV^+−C_{60}^- ($R_{cc} = 15.4$ Å).[31] The reduction of the electronic coupling V, caused by the longer distance between the centers of positive and negative charge density in OAn^+−OPV−C_{60}^-, is the origin of the increase in lifetime for OAn^+−OPV−C_{60}^- compared to OAn−OPV^+−C_{60}^-.

The rate constants of the various photoinduced processes in solvents of different polarity have been calculated using eq 4 relative to the corresponding rate constant in chlorobenzene by assuming that V is independent of the solvent and are collected in Table 4.

Near Steady-State PIA Spectroscopy in the Solid State. Near steady-state PIA spectra of thin films of OPV−C_{60} and OAn−OPV−C_{60} were recorded at 80 K with excitation at 458 nm. The PIA spectrum of the OPV−C_{60} film (Figure 12) exhibits the signals of OPV^+ at 0.68 and 1.52 eV and that of C_{60}^- at 1.24 eV, characteristic of a charge-separated state. The PIA spectrum of a film of OAn−OPV−C_{60} (Figure 12) lacks the bands at 0.68 and 1.52 eV and exhibits only one broad band that peaks at 1.25 eV. This signal is attributed to the overlapping transitions of the OAn^+ and C_{60}^- radical ions and gives evidence

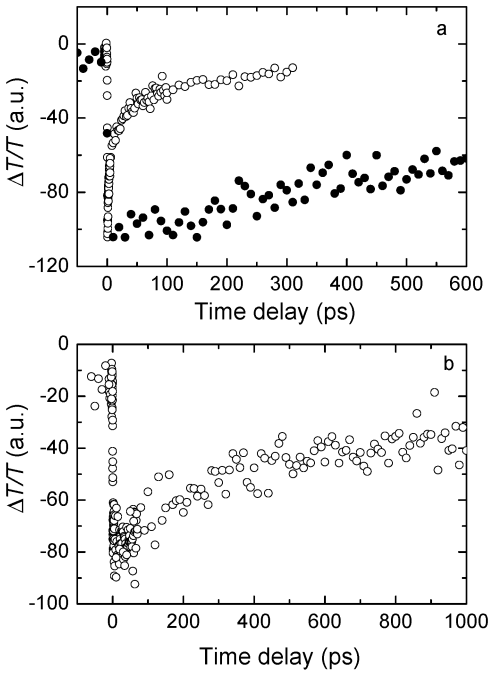

Figure 13. (a) Differential transmission dynamics at 1450 nm of thin films of OAn−OPV−C_{60} (open circles) and OPV−C_{60} (closed circles) at 298 K with excitation at 450 nm. (b) Differential transmission dynamics at 1030 nm of a thin film of OAn−OPV−C_{60} at 298 K with excitation at 450 nm.

for the formation of an intramolecular (OAn−OPV^+−C_{60}^-) or intermolecular (OAn^+−OPV−C_{60}/OAn−OPV−C_{60}^-) charge-separated state. The charge-separated state in the OPV−C_{60} and OAn−OPV−C_{60} films, measured with this PIA technique, extend into the millisecond time domain. The PIA band at 1.25 eV increases with the pump intensity (I) following a square-root power law ($-\Delta T/T \sim I^{0.5}$). This suggests a nongeminate bimolecular recombination of the photoinduced charges. We propose that the long-lived (ms domain) charges observed with near steady-state PIA in films of OPV−C_{60} and OAn−OPV−C_{60} at 80 K are associated with a small fraction of positive and negative charges that have escaped from geminate recombination by charge migration to other sites in the film where they became trapped and are thus associated with different molecules in the film (i.e., OAn^+−OPV−C_{60} and OAn−OPV−C_{60}^-).

Femtosecond Pump−Probe Spectroscopy in the Solid State. Femtosecond spectroscopy shows that in films of OPV−C_{60} and OAn−OPV−C_{60} at room temperature a charge-separated state is formed within 0.5 ps, as evidenced by the instantaneous rise of the 1450 nm differential transmission (Figure 13a) associated with OPV^+ radical cations. Although a lack of higher time-resolution precludes an unambiguous conclusion, we have no evidence that a singlet-energy transfer precedes the electron-transfer reaction in the solid state. Possibly, the photoinduced electron transfer in the solid state is predominantly intermolecular. The OPV^+−C_{60}^- state is much longer lived in the film than in solution (Table 3). This phenomenon has also been observed in other donor−acceptor dyads and has been attributed to the migration of opposite charges to different sites in the film.[8h,9d,32] In contrast, the OPV^+ signal in the film of the triad rapidly decays, with a time constant of 20 ps over the first 100 ps. This is interpreted to result from an intermolecular or intramolecular charge shift (CSH) from OPV^+ to OAn^+. The time profile of the 1030 nm differential transmission (Figure 13b) is consistent with the formation of an OAn^+−OPV−C_{60}^- state in the triad and explains the short lifetime of

the OAn−OPV^+−C_{60}^- state (Figure 13a). This time profile cannot be fitted to monoexponential decay and suggests several lifetimes. This fact can be rationalized by a combination of a direct charge recombination and an indirect charge recombination after migration of the charges in the film.[8h,9d] It should be noticed, however, that contrary to what is observed for the OPV−C_{60} dyad the OAn^+−OPV−C_{60}^- state seems to be longer lived in solution than the OAn^+−OPV−C_{60}/OAn−OPV−C_{60}^- state in the film. As a tentative explanation for this difference, we propose that in solution the triads are isolated from each other such that the weak electronic coupling between the OAn and the C_{60} decelerates the intramolecular charge recombination in OAn^+−OPV−C_{60}^-. In the film, the triads are in intimate contact with each other, and intermolecular charge recombination between OAn^+−OPV−C_{60} and OAn−OPV−C_{60}^- can occur.

Conclusions

We have synthesized a molecular triad, OAn−OPV−C_{60}, with a redox gradient in a linear array. The photophysical processes that may occur in this system are schematically depicted in Figure 4 and have been investigated in solution and in thin films with photoluminescence and transient absorption spectroscopy.

In solution, photoexcitation of either chromophore of the OAn−OPV−C_{60} triad results in an ultrafast (sequence of) singlet-energy transfer (ET, Figure 4) and provides a singlet state on the fulleropyrrolidine unit (OAn−OPV−$^1C_{60}$*), irrespective of the polarity of the solvent. The competitive process of charge separation from the primary ^{1}OAn*−OPV−C_{60} or OAn−^{1}OPV*−C_{60} states are more than 1 order of magnitude slower and were not observed in the triad. In toluene, the singlet OAn−OPV−$^1C_{60}$* state decays via intersystem crossing (ISC) to the OAn−OPV−$^3C_{60}$* triplet state and via PL to the ground state. In more polar solvents, the singlet OAn−OPV−$^1C_{60}$* state gives rise to an intramolecular charge separation reaction (CS) that generates the OAn−OPV^+−C_{60}^- state. The rate for this forward electron-transfer reaction increases with the polarity of the solvent from $k_{CS} = 4.8 \times 10^{10}$ s^{-1} in chlorobenzene to $k_{CS} = 2.0 \times 10^{11}$ s^{-1} in benzonitrile, in qualitative agreement with Marcus theory. Because the oxidation potential of the OAn segment is below that of the OPV unit, the primary OAn−OPV^+−C_{60}^- charge-separated state may undergo an intramolecular redox reaction, or charge shift (CSH), to form OAn^+−OPV−C_{60}^-. The charge recombination in OAn−OPV^+−C_{60}^- (CR1), however, competes with the charge shift. Because the charge recombination is slowed in less polar solvents, the quantum yield for the charge shift is the highest (~0.4) in the least polar solvent in which electron transfer occurs, i.e., chlorobenzene. The charge recombination in the secondary OAn^+−OPV−C_{60}^- charge-separated state (CR2) is significantly slower ($k_{CR2} < 1 \times 10^9$ s^{-1}) than that of the primary OAn−OPV^+−C_{60}^- state ($k_{CR1} = 1.1 \times 10^{10}$ s^{-1}). Hence, the stabilization gained is more than 1 order of magnitude in time. The observed trends in the various rate constants (k_{CS}, k_{CSH}, k_{CR1}, k_{CR2}, k'_{SC}, and k'_{CR}) with changing solvent polarity are in qualitative agreement with Marcus theory when the free energies of the charge-separated states are determined using a continuum model (eq 1).

In thin films, charge generation on the OPV unit of OAn−OPV−C_{60} is much faster ($k_{CS} \geq 3.0 \times 10^{12}$ s^{-1}) and likely predominantly intermolecular. In the films, a subsequent charge-shift occurs from the primary OPV^+ radical cation to an OAn^+ radical cation with a rate close to $k_{CSH} = 5.0 \times 10^{10}$ s^{-1}. Because we consider it likely that in the film the primary charge-separated state involves two molecules, also the charge shift probably involves an intermolecular OAn−OPV^+−C_{60} → OAn^+−OPV−C_{60} reaction, with the negative charge located on the fullerene unit of a third molecule (OAn−OPV−C_{60}^-). The lifetime of the charges formed in the film (OAn^+−OPV−C_{60}/OAn−OPV−C_{60}^-) is somewhat less as compared to the solution.

The experiments on OAn−OPV−C_{60} demonstrate that in solution the OAn−OPV^+−C_{60}^- → OAn^+−OPV−C_{60}^- charge shift and the resulting spatial extension of the charges increase the lifetime of the charge-separated state compared to OAn−OPV^+−C_{60}^-, because the electronic coupling between the redox active groups is strongly reduced. This provides a rationale to explain the long lifetime of the charge-separated state in conjugated polymer:C_{60} blends in terms of charge migration. The major differences in the kinetics of the electron-transfer reactions observed after photoexcitation of OAn−OPV−C_{60} in solution or in thin films further demonstrate that intermolecular interactions are of crucial significance in this respect. Creating and investigating well-defined multichromphoric supramolecular donor−acceptor assemblies, consisting of many judiciously positioned chromophores, will enable a more detailed understanding of photoinduced charge-separation processes in natural and artificial systems.

Experimental Section

All reagents and solvents were used as received or purified using standard procedures. C_{60} was purchased from Bucky, U.S.A. NMR spectra were recorded on a Varian Unity Inova and a Varian Unity Plus at frequencies of 500 and 125 MHz for ^{1}H and ^{13}C nuclei, a Varian Mercury Vx at frequencies of 400 and 100 MHz for ^{1}H and ^{13}C nuclei, or Varian Gemini 2000 at frequencies of 300 and 75 MHz for ^{1}H and ^{13}C nuclei, respectively. Tetramethylsilane (TMS) was used as an internal standard for ^{1}H NMR, and $CDCl_3$, CD_3COCD_3, or CS_2 for was used for ^{13}C NMR. Infrared (FT-IR) spectra were recorded on a Perkin-Elmer Spectrum One UATR FT-IR. Elemental analyses were preformed on a Perkin-Elmer 2400 series II CHN Analyzer. Matrix assisted laser desorption ionization time-of-flight mass spectrometry (MALDI-TOF MS) was performed on a Perseptive DE PRO Voyager MALDI-TOF mass spectrometer using a dithranol matrix. All HPLC analyses were performed on a Hewlett-Packard HP LC−Chemstation 3D (HP 1100 Series) with DAD detection using an Inertsil 5 Si column (250 × 3 mm). A Shimadzu LC-10AT system combined with a Polymer Laboratories MIXED-D column (particle size: 5 μm; length/i.d. (mm): 300 × 7.5) and UV detection were employed for size exclusion chromatography (SEC), using $CHCl_3$ as an eluent (1 mL/min).

(*E*,*E*)-4-{4-(4-Methyl-2,5-bis[(*S*)-2-methylbutoxy]styryl)-2,5-bis[(*S*)-2-methylbutoxy]styryl}-2,5-bis[(*S*)-2-methylbutoxy]}-5-benzaldehyde-dimethylacetal (2). Amberlite IR 120 (1.5 g), trimethyl orthoformate (20 mL), and **1** (1.2 g, 1.78 mmol) were added to 100 mL of methanol. The suspension was stirred under an argon atmosphere at 70 °C for 2 h. The reaction mixture was cooled to room temperature, and 1.5 g of Na_2CO_3 was added. The suspension was filtered, and the solvent was removed in vacuo to yield 1.38 g (91%) of **2**, which was used without further purification.^{1}H NMR ($CDCl_3$, 400 MHz): δ (ppm) 7.50 (d, 1H),7.49 (s, 2H), 7.44 (d, 1H), 7.18 (s, 1H), 7.17 (s, 1H), 7.16 (s, 1H), 7.10 (s, 1H), 7.08 (s, 1H), 6.73 (s, 1H), 3.92−3.74 (m, 12H), 3.42 (s, 6H), 2.24 (s, 3H), 1.98−1.88 (m, 6H), 1.69−1.54 (m, 6H), 1.39−1.26 (m, 6H), 1.10−

0.96 (m, 36 H). ^{13}C NMR ($CDCl_3$, 100 MHz): δ (ppm) 151.69, 151.10, 150.96, 150.67, 150.45, 128.17, 127.71, 127.57, 126.98, 126.56, 125.21, 123.19, 123.06, 122.54, 121.71, 116.32, 111.80, 110.14, 109.94, 109.26, 108.39, 99.75, 74.69, 74.35, 74.28, 74.23, 73.73, 73.38, 54.34, 35.11, 35.08, 35.05, 34.96, 34.89, 26.36, 26.26, 26.21, 16.79, 16.70, 16.40, 11.46, 11.37, 11.33.

***N*-(4-Diphenylaminophenyl)-*N*-phenyl-3-aminobenzaldehyde (4).** To a tube fitted with a magnetic stirrer was added **3** (0.8 g, 2.38 mmol), 3-bromobenzaldehyde (1.32 g, 7.14 mmol), $Pd_2(dba)_3$ (0.022 g, 0.024 mmol), BINAP (0.044 g, 0.071 mmol), and Cs_2CO_3 (1.16 g, 3.57 mmol). After purging with argon, freshly distilled toluene (11.9 mL) was added. The reaction mixture was heated at 100 °C under Ar atmosphere. After 48 h, $Pd_2(dba)_3$ (0.022 g, 0.024 mmol), BINAP (0.044 g, 0.071 mmol), and Cs_2CO_3 (1.16 g, 3.57 mmol) were added, and the mixture was heated for another 72 h. After cooling to room temperature, the reaction mixture was filtered over Celite 545 and concentrated in vacuo. Column chromatography (SiO_2, heptane/CH_2Cl_2 1:1, $R_f = 0.4$) and evaporation to dryness from heptane yielded 0.643 g (62%) of a yellow powder. IR (UATR) ν (cm^{-1}) 3034, 2923, 2851, 1698, 1583, 1485, 1277, 1263, 749, 690, 626. ^{1}H NMR ($CDCl_3$, 400 MHz): δ (ppm) 9.92 (s, 1H), 7.56 (t, 1H), 7.43(dt, 1H), 7.37 (t, 1H), 7.34−7.23 (m, 7H), 7.13−7.11 (m, 6H), 7.08−6.96 (m, 7H). ^{13}C NMR ($CDCl_3$, 100 MHz): δ (ppm) 192.24, 149.14, 148.00, 147.45, 144.17, 142.11, 137.91, 129.98, 129.70, 129.45, 128.18, 126.37, 125.41, 124.62, 124.20, 123.67, 123.07, 122.91, 122.66. Anal. Calcd for $C_{31}H_{24}N_2O$: C, 84.5; H, 5.5; N, 6.4. Found: C, 84.1; H, 5.1; N, 6.1.

***(E)*-*N*,*N*′-(Diphenyl)-*N*′-(4-diphenylaminophenyl)-3-aminobenzaldimine (5).** To a suspension of **4** (0.55 g, 1.24 mmol) in ethanol (50 mL) was added aniline (0.14 g, 1.50 mmol). The reaction mixture was heated at 85 °C for 4 h. After cooling to room temperature, the product precipitated slowly from the ethanol. The product was obtained as 0.508 g (79%) of a yellow powder after washing with ethanol. IR (UATR) ν (cm^{-1}) 3034, 1628, 1589, 1486, 1267, 751, 693. ^{1}H NMR ($CDCl_3$, 400 MHz): δ (ppm) 8.34 (s, 1H), 7.61 (t, 1H), 7.53 (dt, 1H), 7.38−7.31(m, 3H), 7.28−7.10 (m, 16H), 7.03−6.97 (m, 7H). ^{13}C NMR ($CDCl_3$, 100 MHz): δ (ppm) 160.31, 151.99, 148.47, 147.78, 147.56, 143.29, 142.34, 137.40, 129.62, 129.33, 129.19, 129.09, 126.32, 125.91, 125.66, 125.26, 123.95, 123.88, 123.53, 122.82, 122.52, 122.44, 120.85. Anal. Calcd for $C_{37}H_{29}N_3$: C, 86.2; H, 5.7; N, 8.1. Found: C, 85.8; H, 5.3; N, 8.0. MALDI-TOF MS (MW = 515.65) m/z = 515.23 $[M]^+$.

(*E*,*E*,*E*)-4-[4-{4-[*N*-(4-Diphenylaminophenyl)-*N*-(phenyl)-3-aminostyryl]2,5-bis[(*S*)-2-methylbutoxy]styryl}-2,5-bis[(*S*)-2-methylbutoxy]styryl]-2,5-bis[(*S*)-2-methylbutoxy]benzaldehyde (6). Schiff base **5** (0.450 g, 0.873 mmol) and acetal **2** (0.775 g, 0.873 mmol) were dissolved in DMF (5 mL). The mixture was heated to 80 °C under an argon atmosphere, and potassium *tert*-butoxide (0.352 g, 3.142 mmol) was added. The reaction mixture was stirred for 3 h. After cooling to room temperature, the reaction mixture was poured on ice, washed with HCl 3N and brine, dried over $MgSO_4$, and concentrated in vacuo. Column chromatography (SiO_2, toluene/cyclohexane 7:3 $R_f = 0.4$, and heptane/CH_2Cl_2 6:2, $R_f = 0.2$) and evaporation to dryness from heptane yielded 0.795 g (72%) of an orange powder. IR (UATR) ν (cm^{-1}) 3062, 2960, 2917, 2873, 1675, 1589, 1504, 1490, 1422, 1262, 1200, 1039, 968, 744, 693. ^{1}H NMR ($CDCl_3$, 500 MHz): δ (ppm) 10.43(s, 1H), 7.64 (d, 1H), 7.54 (d, 1H), 7.51 (d, 1H), 7.50 (d, 1H), 7.40 (d, 1H), 7.33 (s, 1H), 7.28−6.98 (m, 29H), 3.79 3.98 (m, 12H), 1.98−1.91 (m, 6H), 1.70−1.57 (m, 6H), 1.39−1.31 (m, 6H), 1.13−0.94 (m, 36H). ^{13}C NMR ($CDCl_3$, 100 MHz): δ (ppm) 189.06, 156.43, 151.44, 151.26, 151.04, 150.64, 148.21, 147.84, 142.91, 142.70, 139.13, 135.22, 129.45, 129.19, 129.18, 128.50, 128.45, 127.45, 126.74, 126.48, 126.42, 125.46, 125.30, 123.97, 123.79, 123.74, 123.56, 123.19, 122.98, 122.56, 122.43, 122.40, 122.21, 121.90, 120.29, 110.64, 110.29, 110.17, 109.82, 109.74, 109.64, 74.39, 74.25, 74.11, 74.05, 73.91, 73.69, 35.13, 35.01, 34.93, 34.88, 34.84, 26.38, 26.34, 26.33, 26.18, 16.88, 16.86, 16.81, 16.76, 16.63, 11.52, 11.46, 11.38, 11.32. Anal. Calcd for $C_{85}H_{102}N_2O_7$: C, 80.8; H, 8.1; N, 2.2. Found: C, 80.7; H, 7.6; N, 2.2. MALDI-TOF MS (MW = 1263.75) m/z = 1263.71 $[M]^+$.

***N*-Methyl-2-⟨4-[4-{4-[*N*′-(4-diphenylaminophenyl)-*N*′-(phenyl)]3-aminostyryl]-2,5-bis[(*S*)-2-methylbutoxy]styryl}-2,5-bis[(*S*)-2-methylbutoxy]styryl]-2,5-bis[(*S*)-2-methylbutoxy]⟩-3,4-fulleropyrrolidine (7).** A solution of aldehyde **6** (0.2 g, 0.158 mmol), finely ground *N*-methylglycine (84.4 mg, 0.949 mmol), and C_{60} (227 mg, 0.316 mmol) in chlorobenzene (60 mL) was stirred and refluxed in the dark under an atmosphere of dry nitrogen for 18 h. After cooling to room temperature, the solvent was removed in vacuo, and the remaining residue was purified by column chromatography on silica gel (toluene/cyclohexane: 2/1, R_f = 0.4) to afford triad **7** as a ∼1/1 mixture of diastereomers according to HPLC (eluent: toluene/cyclohexane 50/50 v/v; flow: 1 mL/min.; peaks at t_r = 9.1 and 10.3 min.). Traces of impurities were effectively removed after a 2nd chromatographic purification on silica gel (CS_2/toluene: 1/0 to 7/3 $R_f = 0.3$) to afford analytically pure material (assay >99.5%) according to HPLC and GPC analysis. The product was precipitated from a concentrated toluene solution with methanol (100 mL), and the resulting solid was washed with methanol (2 × 100 mL) and finally dried in vacuo at 55 °C. The triad was obtained as a light brown powder (137 mg, 43%). IR (UATR) ν (cm^{-1}) 2957, 2914, 2872, 1589, 1502, 1491, 1264, 1190, 965, 750, 694, 526. ^{1}H NMR (CS_2, 500 MHz): δ (ppm) 7.61−6.96 (m, 35H), 5.62 (s, 1H), 5.05 (d, 1H), 4.41 (d, 1H), 4.15−3.70 (m, 12H), 2.92 (s, 3H), 2.16−1.26 (m, 18H), 1.02−1.26 (m, 36H). ^{13}C NMR (CS_2, 125 MHz): δ (ppm) 156.50, 154.91, 154.84, 154.18, 154.15, 153.53, 151.61, 150.93, 150.76, 150.71, 150.67, 150.63,147.79, 147.40, 147.06, 146.60, 146.57, 146.52, 146.13, 146.07, 146.03, 146.00, 145.93, 145.89, 145.85, 145.75, 145.50, 145.47, 145.37, 145.26, 145.19, 145.07, 145.04, 145.01, 144.98, 144.91, 144.50, 144.37, 144.31, 144.15, 142.92, 142.86, 142.51, 142.46, 142.43, 142.40, 142.35, 142.12, 142.10, 142.06, 141.99, 141.98, 141.95, 141.92, 141.79, 141.63, 141.53, 141.51, 140.06, 139.98, 139.69, 139.51, 139.07, 136.35, 135.99, 135.88, 135.86, 134.49, 134.44, 129.42, 129.20, 129.17, 127.99, 127.68, 127.66, 127.40, 127.27, 126.88, 126.30, 125.24, 125.14, 124.85, 124.80, 123.79, 123.70, 123.61, 123.29, 122.69, 122.56, 122.52, 122.47, 122.29, 121.96, 120.39, 114.29, 114.16, 110.04, 109.63, 109.40, 109.22, 108.71, 108.61, 76.53, 75.43, 75.40, 73.97, 73.91, 73.69, 73.59, 73.52, 73.44, 72.95, 72.91, 69.70, 68.98, 40.02, 35.41, 35.31, 35.29, 35.25, 35.20, 35.18, 35.17, 26.86, 26.84, 26.80, 26.49, 17.14, 17.09, 17.06, 17.02, 17.00, 16.80, 12.04, 12.03, 12.00, 11.94, 11.89, 11.85. Anal. Calcd for $C_{147}H_{107}N_3O_6$: C, 87.7; H, 5.4; N, 2.1. Found: C, 87.8; H, 5.0; N, 2.1. MALDI-TOF MS (MW = 2011.44) m/z = 2011.18 $[M]^+$.

(*E*,*E*)-2-{4-(4-Methyl-2,5-bis[(*S*)-2-methylbutoxy]styryl)-2,5-bis[(*S*)-2-methylbutoxy]styryl}-1,4-bis[(*S*)-2-methylbutoxy]-5-deuteriobenzene (9). *n*-BuLi 1.6 M (0.13 mL, 0.21 mmol) was added dropwise to a solution of **8** (0.15 g, 0.16 mmol) in freshly distilled diethyl ether (3 mL) at −10° C. The reaction mixture was stirred for 5 min. After the addition of D_2O (0.5 mL), the cooling bath was removed, and the reaction mixture

was stirred for 2 h at room temperature. The mixture was estracted with diethyl ether dried over $MgSO_4$ and concentrated in vacuo. Column chromatography (SiO_2; heptane/CH_2Cl_2: 1/1, $R_f = 0.3$) and recrystallization from ethanol yielded 54 mg (41%) of the product as yellow crystals. ^{1}H NMR ($CDCl_3$, 400 MHz): δ (ppm) 7.49 (d, 1H), 7.48 (s, 2H), 7.44 (d, 1H), 7.19-(s, 1H), 7.18 (s, 1H), 7.17 (s, 1H), 7.10 (s, 1H), 6.82 (s, 1H), 6.72(s, 1H), 3.92−3.71 (m, 12H), 1.99−1.82 (m, 6H), 1.68−1.54 (m, 6H), 1.38−1.23 (m, 6H), 1.20−0.86 (m, 36H). ^{13}C NMR ($CDCl_3$, 100 MHz): δ (ppm) 151.68, 151.14, 150.94, 150.90, 150.44, 128.21, 127.61, 127.54, 127.10, 125.23, 123.24, 122.98, 122.82, 121.74, 116.31, 113.96, 111.58, 110.36, 109.85, 108.34, 74.68, 74.46, 74.30, 74.26, 73.59, 73.38, 35.11, 35.06, 35.04, 34.97, 34.80, 26.36, 26.34, 26.26, 26.19, 16.80, 16.70, 16.56, 16.40, 11.46, 11.40, 11.37, 11.31. Anal. Calcd for $C_{53}H_{79}DO_6$: C, 77.8; H, 10.2. Found: C, 77.5; H, 9.1. MALDI-TOF MS (MW = 813.96) $m/z = 813.53[M]^+$.

(*E*,*E*,*E*)-2-[4-{4-[*N*-(4-Diphenylaminophenyl)-*N*-(phenyl)-3-aminostyryl]-2,5-bis[(*S*)-2-methylbutoxy]styryl}-2,5-bis-[(*S*)-2-methylbutoxy]styryl]-1,4-bis[(*S*)-2-methylbutoxy]-5-deuteriobenzene (10). Schiff base **5** (0.025 g, 0.049 mmol) and **9** (0.40 g, 0.049 mmol) were dissolved in DMF (5 mL). The mixture was heated at 80 °C under an argon atmosphere, and potassium *tert*-butoxide (0.020 g, 0.176 mmol) was added. The reaction mixture was stirred for 5 h at 80 °C. After cooling to room temperature, the reaction mixture was poured onto ice and washed with HCl 3 N and brine. The organic layer was dried over $MgSO_4$ and concentrated in vacuo. Column chromatography (SiO_2, toluene/cyclohexane 7:3, $R_f = 0.6$) and recyrstallization from hexane, heptane, and a few drops of CH_2Cl_2 yielded 30 mg of **10** (50%) as a yellow powder. IR (UATR) ν (cm^{-1}) 2960, 2917, 2873, 1588, 1504, 1489, 1255, 1205, 1042, 970, 744, 693. ^{1}H NMR (CD_3COCD_3, 400 MHz): δ (ppm) 7.61 (s, 2H), 7.60 (d, 1H), 7.55 (d, 1H), 7.47(d, 1H), 7.35−6.95 (m, 30H), 4.01−3.76 (m, 12H), 2.09−1.83 (m, 6H), 1.74−1.55 (m, 6H), 1.45−1.26 (m, 6H), 0.95−1.15 (m, 36H), ^{13}C NMR (100 MHz): δ (ppm) 155.25, 152.89, 152.84, 152.72, 150.10, 149.58, 149.54, 144.87, 144.58, 141.06, 131.32, 131.03, 130.98, 130.19, 129.47, 129.13, 128.96, 128.91, 128.15, 127.30, 127.04, 125.39, 125.35, 125.16, 124.93, 124.87, 124.73, 124.68, 124.37, 124.34, 124.30, 123.17, 122.16, 115.71, 113.14, 112.34, 111.95, 111.58, 111.39, 75.61, 75.56, 75.53, 75.36, 74.72, 36.76, 36.68, 36.63, 36.44, 27.85, 27.81, 27.60, 18.04, 17.98, 17.95, 17.92, 17.60, 12.63, 12.60, 12.58, 12.52, 12.39. Anal. Calcd for $C_{85}H_{102}N_2O_7$: C,81.6; H, 8.2; N, 2.3. Found: C, 81.2; H, 7.7; N, 2.2. MALDI-TOF MS (MW = 1236.74) $m/z = 1235.62$ $[M]^+$.

Electrochemistry. Cyclic voltammograms were measured in 0.1 M tetrabutylammonium hexafluorophosphate ($TBAPF_6$) as a supporting electrolyte in dichloromethane (or THF) using a Potentioscan Wenking POS73 potentiostat. The working electrode was a Pt disk (0.2 cm^2), the counter electrode was a Pt plate (0.5 cm^2), and a saturated calomel electrode (SCE) was used as reference electrode, calibrated against Fc/Fc^+ (+0.43 V).

Absorption and Photoluminescence. UV/visible/near-IR absorption spectra were recorded on a Perkin-Elmer Lambda 900 spectrophotometer. Fluorescence spectra were recorded on an Edinburgh Instruments FS920 double-monochromator spectrometer and a Peltier-cooled red-sensitive photomultiplier.

Time-Correlated Single Photon Counting. Time-correlated single photon counting fluorescence studies were performed using an Edinburgh Instruments LifeSpec-PS spectrometer. The LifeSpec-PS comprises a 400 nm picosecond laser (PicoQuant PDL 800B) operated at 2.5 MHz and a Peltier-cooled Hamamatsu microchannel plate photomultiplier (R3809U-50). Lifetimes were determined from the data using the Edinburgh Instruments software package.

Near Steady-State PIA. Solutions were prepared in a nitrogen-filled glovebox in order to exclude interference of oxygen during measurements. The PIA spectra were recorded between 0.5 and 3.0 eV by excitation with a mechanically modulated cw Ar ion laser ($\lambda = 458$ or 528 nm, 275 Hz) pump beam and monitoring the resulting change in transmission of a tungsten−halogen probe light through the sample (ΔT) with a phase-sensitive lock-in amplifier after dispersion by a grating monochromator and detection, using Si, InGaAs, and cooled InSb detectors. The pump power incident on the sample was typically 25 mW with a beam diameter of 2 mm. The PIA ($-\Delta T/T \approx \Delta$O.D.) was directly calculated from the change in transmission after correction for the PL, which was recorded in a separate experiment. PIA and PL spectra were recorded with the pump beam in a direction almost parallel to the direction of the probe beam. The solutions were studied in a 1 mm near-IR grade quartz cell at room temperature. Solvents for PIA measurements were distilled under nitrogen before use. The solid-state measurements were performed on films, drop cast from chloroform solution on quartz substrate, and held at 80 K in an Oxford continuous flow cryostat.

Transient Subpicosecond Photoinduced Absorption. The femtosecond laser system used for pump−probe experiments consists of an amplified Ti/sapphire laser (Spectra Physics Hurricane). The single pulses from a cw mode-locked Ti/sapphire laser were amplified by a Nd:YLF laser using chirped pulse amplification, providing 150 fs pulses at 800 nm with an energy of 750 μJ and a repetition rate of 1 kHz. The pump pulses at 450 nm were created via optical parametric amplification (OPA) of the 800 nm pulse by a BBO crystal into infrared pulses which were then two times frequency doubled via BBO crystals. The probe beam was generated in a separate optical parametric amplification setup in which 1030 and 1450 nm pulses were created. The pump beam was focused to a spot size of about 1 mm^2 with an excitation flux of 1 mJ cm^{-2} per pulse. For the 1030 and 1450 nm pulses a RG 850 nm cutoff filter was used to avoid contributions of residual probe light (800 nm) from the OPA. The probe beam was reduced in intensity compared to the pump beam by using neutral density filters of OD = 2. The pump beam was linearly polarized at the magic angle of 54.7° with respect to the probe, to cancel out orientation effects in the measured dynamics. The temporal evolution of the differential transmission was recorded using Si or an InGaAs detector by a standard lock-in technique at 500 Hz. Solutions in the order of $2-5 \times 10^{-4}$ M were excited at 450 nm, i.e., providing primarily excitation of the OPV part within the molecules. The solid-state measurements were performed on films, drop cast from chloroform solution.

Acknowledgment. This research has been supported by the Dutch Ministry of Economic Affairs, the Ministry of Education, Culture and Science, and the Ministry of Housing, Spatial Planning, and the Environment through the E.E.T. program (EETK97115). The research in Eindhoven has also been supported by The Netherlands Organization for Scientific Research (NWO) and the Eindhoven University of Technology through a grant in the PIONIER program. The research of S. C. J. Meskers has been made possible by a fellowship of the Royal Netherlands Academy of Arts and Sciences.

Supporting Information Available: Further details of the mathematical modeling. This material is available free of charge via the Internet at http://pubs.acs.org.

References and Notes

(1) (a) *The Photosynthetic Reaction Center*; Deisenhofer, J., Norris, J. R., Eds.; Academic Press: New York, 1993. (b) *Anoxygenic Photosynthetic Bacteria*; Blankenschip, R. E., Madigan, M. T., Bauer, C. E., Eds.; Kluwer Academic Publishers: Dordrecht, The Netherlands, 1995.

(2) (a) *Molecular Electronics*; Jortner, J., Ratner, M. Eds.; Blackwell: London, 1997. (b) Lehn, J.-M. *Supramolecular Chemistry*; VCH: Weinheim, Germany, 1995. (c) *Electron Transfer in Chemistry Vol. I*−*IV*; Balzani, V., Ed.; Wiley-VCH: Weinheim, Germany, 2001.

(3) Tang, C. W. *Appl. Phys. Lett.* **1986**, *48*, 183.

(4) (a) Nunzi, J.-M.*C. R. Physique* **2002**, *3*, 523. (b) Nelson, J. *Curr. Opin. Solid State Mater. Sci*. **2002,** *6*, 87.

(5) (a) Sariciftci, N. S.; Smilowitz, L.; Heeger, A. J.; Wudl, F. *Science* **1992**, *258*, 1474. (b) Yu, G.; Gao, J.; Hummelen, J. C.; Wudl, F.; Heeger, A. J. *Science* **1995**, *270*, 1789.

(6) (a) Kraabel, B.; McBranch, D.; Sariciftci, N. S.; Moses, D.; Heeger, A. J. *Phys. Rev. B* **1994**, *50*, 18543. (b) Kraabel, B.; Hummelen, J. C.; Vacar, D.; Moses, D.; Sariciftci, N. S.; Heeger, A. J. *J. Chem. Phys.* **1996**, *104*, 4267. (c) Brabec, C. J.; Zerza, G.; Cerullo, G.; De Silvestri, S.; Luzatti, S.; Hummelen, J. C.; Sariciftci, N. S. *Chem. Phys. Lett.* **2001**, *340*, 232.

(7) (a) Smilowitz, L.; Sariciftci, N. S.; Wu, R.; Gettinger, C.; Heeger, A. J.; Wudl, F. *Phys. Rev. B* **1993**, *47*, 13835. (b) Meskers, S. C. J.; van Hal, P. A.; Spiering, A. J. H.; van der Meer, A. F. G.; Hummelen, J. C.; Janssen, R. A. J. *Phys. Rev. B.* **2000**, *61*, 9917. (c) Montanari, I.; Nogueira, A. F.; Nelson, J.; Durrant, J.; Loi, M.-A.; Winder, C.; Sariciftci, N. S.; Brabec, C. J. *Appl. Phys. Lett.* **2002**, *81*, 3001.

(8) Oligothiophene-fullerene dyads: (a) Benincori, T.; Brenna, E.; Sannicolo, F.; Trimarco, L.; Zotti, G.; Sozzani, P. *Angew. Chem., Int. Ed. Engl.* **1996**, *35*, 648. (b) Effenberger; F.; Grube, G. *Synthesis* **1998**, 1372. (c) Knorr, S.; Grupp, A.; Mehring, M.; Grube, G.; Effenberger, F. *J. Chem. Phys.* **1999**, *110*, 3502. (d) Yamashiro, T.; Aso, Y.; Otsubo, T.; Tang, H.; Harima, Y.; Yamashita, K. *Chem. Lett.* **1999**, 443. (e) Fujitsuka, M.; Ito, O.; Yamashiro, T.; Aso, Y.; Otsubo, Y. *J. Phys. Chem. A* **2000**, *104*, 4876. (f) van Hal, P. A.; Knol, J.; Langeveld-Voss, B. M. W.; Meskers, S. C. J.; Hummelen, J. C.; Janssen, R. A. J. *J. Phys. Chem. A* **2000**, *104*, 5974. (g) van Hal, P. A.; Janssen, R. A. J.; Lanzani, G.; Cerullo, G.; Zavelani-Rossi, M.; De Silvestri, S. *Chem. Phys. Lett.* **2001**, *345*, 33. (h) Fujitsuka, M.; Masahura, A.; Kasai, H.; Oikawa, H.; Nakanishi, H.; Ito, O.; Yamashiro, T.; Aso, Y.; Otsubo, T. *J. Phys. Chem. B* **2001**, *105*, 9930. (i) Fujitsuka, M.; Matsumoto, K.; Ito, O.; Yamashiro, T.; Aso, Y.; Otsubo, T. *Res. Chem. Intermed.* **2001**, *27*, 73. (j) Hirayama, D.; Takimiya, K.; Aso, Y.; Otsubo, T. Hasobe, T.; Yamada, H. Imahori, H.; Fukuzumi, S.; Sakata, Y. *J. Am. Chem. Soc.* **2002**, *124*, 532.

(9) Oligo(*p*-phenylene vinylene)-fullerene dyads: (a) Nierengarten, J. F.; Eckert, J. F.; Nicoud, J. F.; Ouali, L.; Krasnikov, V.; Hadziioannou, G. *Chem. Commun.* **1999**, 617. (b) Eckert, J. F.; Nicoud, J. F.; Nierengarten, J. F.; Liu, S. G.; Echegoyen, L.; Barigelletti, F.; Armaroli, N.; Ouali, L.; Krasnikov, V. V.; Hadziioannnou, G. *J. Am. Chem. Soc.* **2000**, *122*, 7467. (c) Armaroli, N.; Barigelletti, F.; Ceroni, P.; Eckert, J.-F.; Nicoud, J.-F.; Nierengarten, J.-F. *Chem. Commun.* **2000**, 599. (d) Peeters, E.; van Hal, P. A.; Knol, J.; Brabec, C. J.; Sariciftci, N. S.; Hummelen, J. C.; Janssen, R. A. J. *J. Phys. Chem. B* **2000**, *104*, 10174. (e) van Hal, P. A.; Janssen, R. A. J.; Lanzani, G.; Cerullo, G.; Zavelani-Rossi, M.; De Silvestri, S. *Phys. Rev. B* **2001**, *64*, 075206. (f) Nierengarten, J.-F.; Armaroli, N.; Accorsi, G.; Rio, Y.; Eckert, J.-F. *Chem. Eur. J.* **2003**, *9*, 37.

(10) Oligo(thienylene vinylene)-fullerene dyads: (a) Liu, S.-G.; Shu, L.; Rivera, J.; Liu, H.; Raimundo, J.-M.; Roncali, J.; Gorgues, A.; Echegoyen, L. *J. Org. Chem.* **1999**, *64*, 4884. (b) Liu, S.-G.; Martineau, C.; Raimundo, J.-M.; Roncali, J.; Echegoyen, L. *Chem. Commun.* **2001**, 913. (c) Martineau, C.; Blanchard, P.; Rondeau, D.; Delaunay, J.; Roncali, J. *Adv. Mater.* **2002**, *14*, 283. (d) Apperloo, J. J.; Martineau, C.; van Hal, P. A.; Roncali, J.; Janssen, R. A. J. *J. Phys. Chem. A* **2002**, *106*, 21.

(11) Oligoene-fullerene dyads: (a) Imahori, H.; Cardoso, S.; Tatman, D.; Lin, S.; Noss, L.; Seely, G. R.; Sereno, L.; Chessa de Silber, J.; Moore, T. A.; Moore, A. L.; Gust, D. *Photochem. Photobiol.* **1995**, *62*, 1009. (b) Yamazaki, M.; Araki, Y.; Fuijtsuha, M.; Ito, O. *J. Phys. Chem. A* **2001**, *105*, 8615.

(12) Miscellaneous: oligomer-fullerene dyads: (a) Segura, J. L.; Gómez, R.; Martín, N.; Luo, C.; Guldi, D. M. *Chem. Commun.* **2000**, 701. (b) Guldi, D. M.; Swartz, Luo, C.; Gómez, R.; Segura, J. L.; Martín, N. *J. Am. Chem. Soc.* **2002**, *124*, 10875. (c) Guldi, D. M.; Luo, C.; Schwartz, A.; Gómez, R.; Segura, J. L.; Martin, N.; Brabec, C. J.; Sariciftci, N. S. *J. Org. Chem.* **2002**, *67*, 1141. (d) Gu, T.; Tsamouras, D.; Melzer, C.; Krasnikov, V.; Gisselbrecht, J.-P.; Gross, M.; Hadziioannou, G.; Nierengarten, J.-F. *Chem. Phys. Chem.* **2002**, 124.

(13) van Hal, P. A.; Beckers, E. H. A.; Meskers, S. C. J.; Janssen, R. A. J.; Jousselme, B.; Blanchard, P.; Roncali, J. *Chem. Eur. J.* **2002**, *8*, 5415.

(14) For recent reviews, see: (a) Gust, D.; Moore, T. A.; Moore, A. L. *Acc. Chem. Res.* **2001**, *34*, 40. (b) Guldi, D. M. *Chem. Soc. Rev.* **2002**, *31*, 22.

(15) (a) Liddell, P. A.; Kuciauskas, D.; Sumida, J. P.; Nash, B.; Nguyen, D.; Moore, A. L.; Moore, T. A.; Gust, D. *J. Am. Chem. Soc.* **1997**, *119*, 1400. (b) Imahori, H.; Yamada, K.; Hasegawa, M.; Taniguchi, S.; Okada, T.; Sakata, Y. *Angew. Chem., Int. Ed. Engl.* **1997**, *36*, 2626. (c) Carbonera, D.; Di Valentin, M.; Corvaja, C.; Agostini, G.; Giacometti, G.; Liddell, P. A.; Kuciauskas, D.; Moore, A. L.; Moore, T. A.; Gust, D. *J. Am. Chem. Soc.* **1998**, *120*, 4398. (d) Kuciauskas, D.; Liddell, P. A.; Moore, A. L.; Moore, T. A.; Gust, D. *J. Am. Chem. Soc.* **1998**, *120*, 10880. (e) Tamaki, K.; Imahori, H.; Sakata, Y.; Nishimura, Y.; Yamazaki, I. *Chem. Commun.* **1999**, 625. (f) Imahori, H.; Yamada, H.; Ozawa, S.; Sakata, Y.; Ushida, K. *Chem. Commun.* **1999**, 1165. (g) Fujitsuka, M.; Ito, O.; Imahori, H.; Yamada, K.; Yamada, H.; Sakata, Y. *Chem. Lett.* **1999**, 721. (h) Imahori, H.; Yamada, H.; Nishimura, Y.; Yamazaki, I.; Sakata, Y. *J. Phys. Chem. B* **2000**, *104*, 2099. (i) Kuciauskas, D.; Liddell, P. A.; Lin, S.; Stone, S. G.; Moore, A. L.; Moore, T. A.; Gust, D. *J. Phys. Chem. B* **2000**, *104*, 4307. (j) Luo, C.; Guldi, D. M.; Imahori, H.; Tamaki, K.; Sakata, Y *J. Am. Chem. Soc.* **2000**, *122*, 6535. (k) Imahori, H.; Tamaki, K.; Yamada, H.; Yamada, K.; Sakata, Y.; Nishimura, Y.; Yamazaki, I.; Fujitsuka, M.; Ito, O. *Carbon* **2000**, *38*, 1599. (l) Bahr, J. L.; Kuciauskas, D.; Liddell, P. A.; Moore, A. L.; Moore, T. A.; Gust, D. *Photochem. Photobiol.* **2000**, *72*, 598. (m) Imahori, H.; Norieda, H.; Yamada, H.; Nishimura, Y.; Yamazaki, I.; Sakata, Y.; Fukuzumi, S. *J. Am. Chem. Soc*. **2001**, *123*, 100. (n) Fukuzumi, S.; Imahori, H.; Yamada, H.; El-Khouly, M. E.; Fujitsuka, M.; Ito, O.; Guldi, D. M. *J. Am. Chem. Soc. **2001**, 123*, 2571. (o) Imahori, H.; Tamaki, K.; Guldi, D. M.; Luo, C.; Fujitsuka, M.; Ito, O.; Sakata, Y.; Fukuzumi, S. *J. Am. Chem. Soc.* **2001**, *123*, 2607. (p) Imahori, H.; Guldi, D. M.; Tamaki, K.; Yoshida, Y.; Luo, C.; Sakata, Y.; Fukuzumi, S. *J. Am. Chem. Soc.* **2001**, *123*, 6617. (q) Fukuzumi, S.; Imahori, H.; Okamoto, K.; Yamada, H.; Fujitsuka, M.; Ito, O.; Guldi, D. M. *J. Phys. Chem. A* **2002**, *106*, 1903. (r) Liddell, P. A.; Kodis, G.; De la Garza, L.; Bahr, J. L.; Moore, A. L.; Moore, T. A.; Gust, D. *Helv. Chim. Acta* **2001**, *84*, 2765. (s) Ikemoto, J.; Takimiya, K.; Aso, Y.; Otsubo, T.; Fujitsuka, M.; Ito, O. *Org. Lett.* **2002**, *4*, 309. (t) Imahori, H.; Tamaki, K.; Araki, Y.; Hasobe, T.; Ito, O.; Shimomura, A.; Kundu, S.; Okada, T.; Sakata, Y.; Fukuzumi, S. *J. Phys. Chem. A* **2002**, *106*, 2803. (u) Imahori, H.; Tamaki, K.; Araki, Y.; Sekiguchi, Y.; Ito, O.; Sakata, Y.; Fukuzumi, S. *J. Am. Chem. Soc.* **2002**, *124*, 5165. (v) D'Souza, F.; Deviprasad, G. R.; Zandler, M. E.; El-Khouly, M. E.; Fujitsuka, M.; Ito, O. *J. Phys. Chem. B* **2002**, *106*, 4952. (w) Liddell, P. A.; Kodis, G.; Moore, A. L.; Moore, T. A.; Gust, D. *J. Am. Chem. Soc*. **2002**, *124*, 7668. (x) Kodis, G.; Liddell, P. A.; de la Garza, L.; Moore, A. L.; Moore, T. A.; Gust, D. *J. Mater. Chem.* **2002**, *12*, 2100.

(16) Strohrieghl, P.; Jesberger, G.; Heinze, J.; Moll, T. *Makromol. Chem.* **1992**, *193*, 909.

(17) (a) Siegrist, A. E. *Helv. Chim. Acta* **1967**, *50*, 906. (b) Siegrist, A. E.; Meyer, H. R.; Weber, K. *Helv. Chim. Acta* **1969**, *52*, 2521.

(18) Murata, Y.; Shine, H. J. *J. Org. Chem.* **1969**, *34*, 3368.

(19) van Meurs, P. J. High-Spin Molecules of *p*-Phenylenediamnine Radical Cations, Ph.D. Thesis, Eindhoven University of Technology, Eindhoven, The Netherlands, 2002.

(20) van Hal, P. A.; Beckers, E. H. A.; Peeters, E.; Apperloo, J. J.; Janssen, R. A. J. *Chem. Phys. Lett.* **2000**, *328*, 403.

(21) Weller, A. *Z. Phys. Chem. Neue Folge* **1982**, *133*, 93.

(22) The assumption that charges are located at the centers is of course a simplification of the actual situation in which charges are delocalized. Especially for C_{60}, the charges are not expected to be at the center but rather at the outer surface.

(23) The PL lifetime of the residual emission at 510 nm contained a contribution of long lifetime (∼1 ns) and is in part attributed to residual PL emission by minor impurities in the sample.

(24) In toluene, the energy level of the initial charge separated state [OAn−OPV^{+}−C_{60}^{-}] is higher than that of OAn−OPV−$^{1}C_{60}$* due to the destabilization in the nonpolar solvent. In such a case, one can also expect that initial electron transfer from ^{1}OPV* to C_{60} occurs to yield OAn−OPV^{+}−C_{60}^{-}, which subsequently recombines to generate OAn−OPV−$^{1}C_{60}$*. The stepwise pathway would compete with the direct energy transfer pathway from ^{1}OPV* to C_{60} to produce the same state. However, in view of the high rate of the energy transfer (190 fs), it is very unlikely that this process occurs and the same rate of 190 fs has been found in ODCB, where the OAn−OPV^{+}−C_{60}^{-} state is below the OAn−OPV−$^{1}C_{60}$* state (ref 9e).

(25) The function $f(t) = a_0(\exp(-a_1(t - a_3)) - \exp(-a_2(t - a_3)) + a_4)$ was used to fit the data, and all 5 parameters (a_0 − a_4) were optimized.

(26) (a) Wasielewski, M. R.; Niemczyk, M. P.; Svec, W. A.; Pewitt, E. B. *J. Am. Chem. Soc.* **1985**, *107*, 1080. (b) Asahi, T.; Ohkohchi, M.; Matsusaka, R.; Mataga, N.; Zhang, R. P.; Osuka, A.; Maruyama, K. *J. Am. Chem. Soc.* **1993**, *115*, 5665. (c) Macpherson, A. N.; Liddell, P. A.; Lin, S.; Noss, L.; Seely, G. R.; DeGraziano, J. M.; Moore, A. L.; Moore, T. A.; Gust, D. *J. Am. Chem. Soc.* **1995**, *117*, 7202. (d) Kroon, K.; Verhoeven, J. W.; Paddon-Row: M. N.; Oliver, A. M. *Angew. Chem Int. Ed. Engl.* **1991**, *30*, 1358. (e) Imahori, H.; El-Khouly, M. E.; Fujitsuka, M.; Ito, O.; Sakata, Y.; Fukuzumi S. *J. Phys. Chem. A* **2001**, *105*, 325.

(27) Guldi, D. M.; Prato, M. *Acc. Chem. Res.* **2000**, *33*, 695.
(28) Because the experimental data (Figure 9, open circles) show no decay in the first nanosecond, a fit of the lifetime of the $OAn^{+}-OPV-C_{60}^{-}$ state cannot give a reliable value. In the absence of a decay, we have arbitrarily set $k_{CR2} = 0\ s^{-1}$. Further details are described in the Supporting Information.
(29) Deussen, M.; Bässler, H. *Chem. Phys.* **1992**, *164*, 247.
(30) Jortner, J. *J. Chem. Phys.* **1976**, *64*, 4860.
(31) Imahori et. al. reported that the electronic coupling in a triad (0.019 cm^{-1}) is much less compared to that in a dyad (3.9 cm^{-1}), see ref 15o.
(32) (a) Thomas, K. G.; Biju, V.; Guldi, D. M.; Kamat, P. V. George, M. V. *J. Phys. Chem. B* **1999**, *103*, 8864. (b) Imahori, H.; Hasobe, T.; Yamada, H.; Kamat, P. V.; Barazzouk, S.; Fujitsuka, M.; Ito, O.; Fukuzumi, S. *Chem. Lett.* **2001**, 784.